Responses to Reviewer #2

Wang et al paper presents, compared and discusses a set of complementary remote sensing, contact and non-contact in-situ ground deformation measurements acquired at two sites on the Tibetan Plateau. A such diversity and long record of collocated observations is rare in permafrost terrain. I congratulate the authors on the effort to acquire, analyse and disseminate these results. I believe the dataset and the study are definitively valuable and that the article is worth publication after minor revisions. I have no major concern regarding the content but I suggest several ideas to enhance the value of the work and improve the readability of the paper.

We sincerely thank the reviewer for the positive assessment of our work and for the thorough and constructive comments. We have carefully addressed each comment and revised the manuscript accordingly. These suggestions have helped us improve the completeness, clarity, and readability of the manuscript. Detailed responses to the individual comments are provided below.

• **Data availability:** l.694-695 only mention how to access the unprocessed radar images, which seems to indicate that the data record is not openly available yet. Given the uniqueness of the observations, I hope the authors have planned to provide the full data series in an open repository. This might be valuable for many other researchers on the way further!

The deformation records from the supersite for the period from 18 June 2022 to 5 February 2026, including surface soil temperature, daily LVDT deformation time series, raw and smoothed daily ultrasonic ranging data, and raw and smoothed daily GNSS-IR data, have been uploaded to Zenodo. We plan to make these records publicly available upon publication of the article.

• **Additional background information and processing details:** Sections 2 and 3 could benefit from additional details. In addition, some information is currently scattered/hidden in other sections (results and discussion). It would be easier for the reader to get them from the beginning. Some examples thereafter:

Thank you for these suggestions. We have introduced the site background information earlier in the manuscript, added details of data quality control, expanded the information on InSAR baselines and interferogram statistics. Detailed responses to each comment are provided below.

• Section 2: A brief intro about the soil type, grain size, expected ice content/type at different depths, and the potential differences between the two sites would be valuable to understand some of our interpretation in the

following. Such info comes very late in the manuscript (e.g., l. 612-616). Before that, we are missing a bit of context.

Thank you for this suggestion. We have added background information on both sites and their ground ice conditions to the Study area section, as follows:

2 Study area and measurement sites

Borehole drilling conducted during the Second Tibetan Plateau Scientific Expedition in November 2019 provided the foundation for subsequent permafrost observations. By this time of year, seasonal thaw is generally expected to have reached its maximum depth. The 2019 field records document contrasting surface conditions at the two sites. Site SLC03 occupies a flat valley floor supporting alpine swamp meadow, with approximately 90 % vegetation cover, locally degraded frost-heave hummocks, and exposed gravel. SLC07 is situated in degraded alpine meadow with sparse vegetation, a dry, sandy surface containing gravel, and pronounced soil salinization. The boreholes reach depths of 30 m at SLC03 and 20 m at SLC07. At SLC03, the drilling log describes fine sand with gravel in the upper meter, underlain by gravelly sand between 1.0 and 4.6 m depth, tentatively interpreted as glaciofluvial deposits. Ice crystals are visible at 2.4–3.0 m, and the core recovered from 3.0–4.5 m contains abundant water and has a slurry-like consistency. Discrete ice layers occur at greater depths, including an approximately 2.5 mm thick layer within 4.6–5.1 m, a 2.8 cm thick pure-ice layer at 7.3–7.4 m, and a 30 cm thick pure-ice layer at 16.0–16.3 m. Volumetric water content in borehole core samples from SLC03 varied substantially across depths of 0.2–29.4 m, with a mean of 0.32 m^3/m^3 and particularly high values of 0.47 and 0.56 m^3/m^3 at 2.7 and 4.6 m, respectively (Appendix Figure A1). Subsequent active layer temperature and moisture profiles indicate an active layer thickness (ALT) of approximately 2.4 m. Together with the drilling records, these observations suggest the presence of excess ice near the top of permafrost. At SLC07, the drilling log describes dry sandy soil at 0–0.7 m, clay at 0.7–1.6 m, and rock at 1.6–3.5 m. Abundant liquid water was observed in the fragmented core recovered from 2.5–3.5 m. Clay containing angular rock fragments occurs at 3.5–6.0 m, where liquid water but no visible ice was recorded. Rock dominates the 6.0–18.0 m interval, with liquid water noted at 6.0–6.5 m, whereas grey clay containing gravel occurs at 18.0–20.0 m, with no visible ice recorded. Volumetric water contents at depths of approximately 0.5, 1.2, and 3.5 m are 0.31, 0.42, and 0.27 m^3/m^3, respectively.

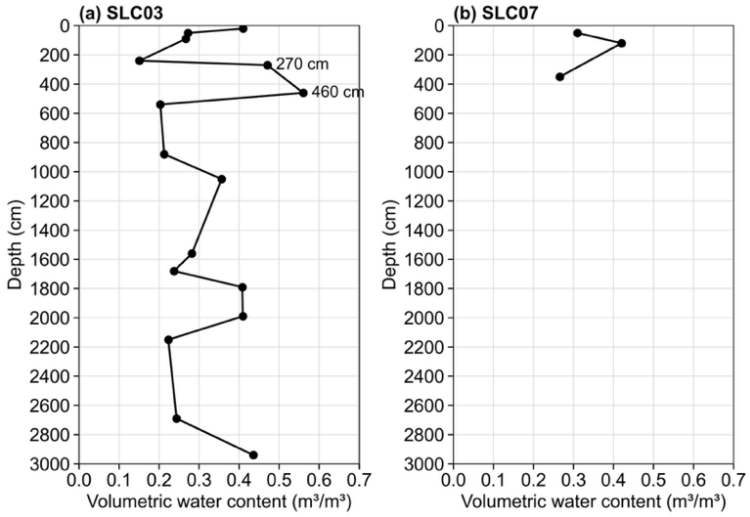


Figure A1. Volumetric water content profiles from borehole core samples collected at (a) SLC03 and (b) SLC07. Black circles denote values at sampling depths.

• Section 3.1: Processing info about the applied filtering / potential outlier removal procedure (similar to Sections 3.2-3.3) are missing.

We have added the following description to Section 3.1:

The LVDT records contained relatively little noise, with only occasional isolated spikes. These outliers were manually reviewed and removed when an observation differed from the preceding value by more than 0.5 mm and the subsequent observation returned to that earlier displacement level. Given the high sampling frequency, the resulting gaps were left unfilled. At SLC03, daily mean displacement was calculated by directly averaging the available high-frequency observations within the selected daily observation window.

• Section 3.2: At l.185, the number/proportion of outliers that were removed could be documented.

The following information has been added to Section 3.2:

The record from 1 June 2022 to 29 November 2025 spanned 1278 days, with observations available on 1096 days and missing on 182 days. Of the available daily observations, 73 (6.66%) were flagged as outliers and removed.

• Section 3.4: Although indirectly mentioned at l. 217-218, it would be good to specific the temporal baseline (12-24d). The corresponding detection capability (max detectable displacement) could also be documented.

The number of used interferograms (and potentially the number of those which have been discarded) could be reported.

We have added the following processing details to **Section 3.4 Sentinel-1 SBAS-InSAR ground surface deformation monitoring**:

For Sentinel-1, the radar wavelength of approximately 5.55 cm corresponds to a LOS displacement of approximately 27.8 mm per complete phase cycle. A total of 250 Sentinel-1 SLC acquisitions were obtained in interferometric wide-swath mode along the ascending track (Path 41) between 5 August 2017 and 15 November 2025. Interferograms were generated by pairing each SAR acquisition with its next two acquisitions (t – t+1 and t – t+2), with temporal baselines generally ranging from 12 to 24 d and occasionally extending to 36 d. This pairing strategy yielded a total of 497 interferometric pairs. SBAS-InSAR processing was performed using ISCE2 and MintPy. During processing, 10 looks in range and 2 looks in azimuth were applied to reduce noise and produce an approximately square grid (finally geocoded to 40 m grid). Differential phases were unwrapped using the SNAPHU minimum cost flow algorithm (C. W. Chen & Zebker, 2002), and the interferogram network was inverted into a deformation time series using a weighted least-squares approach. Following time-series inversion, phase deramping and correction for residual topographic errors were applied. The deformation time series was then smoothed using a three-acquisition moving average, with a nominal window length of 36 d (occasionally 48 d).

In the study area, the land surface is covered by alpine meadow in summer, while winter snow cover is generally thin and short-lived. The relatively sparse vegetation and limited snow cover help maintain relatively high coherence throughout the year in C-band interferometric pairs with temporal baselines of up to one month. Across the 497 interferograms, mean coherence ranges from 0.59 for the 20230506–20230530 interferometric pair to 0.99 for the 20230915–20230927 pair, with 464 interferograms having a mean coherence greater than 0.8. All 497 interferograms are retained in the analysis. Their coherence distribution is presented in Appendix Figure A3.

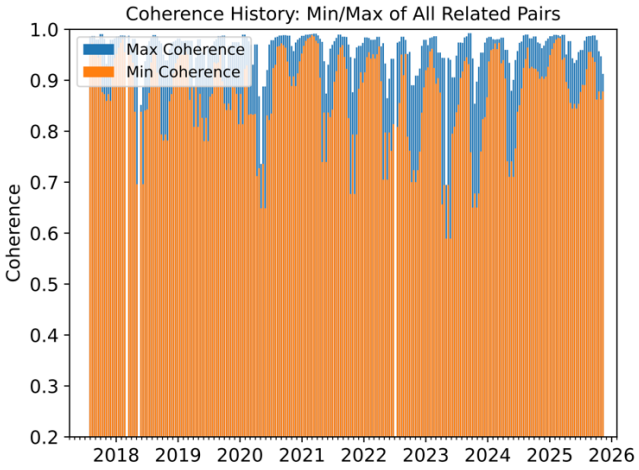


Figure A3. Overview of interferometric coherence: the minimum and maximum mean coherence of all interferogram pairs associated with each acquisition date.

L.224: the moving window is therefore 36 days, right?

Yes. We have clarified the window length in the manuscript as follows: “The deformation time series was then smoothed using a three-acquisition moving average, with a nominal window length of 36 d (occasionally 48 d).”

• Section 3.5: At l.570, it is mentioned that the deepest sensors failed. Good to mention it in Section 3.5 as well, and specify which ones (which depth).

Thank you for this suggestion. We have added the following description to **Section 3.5 Meteorological and active layer hydrothermal monitoring**:

These observations include air temperature at 2 m, precipitation, soil temperature (ST), and soil volumetric water content (VWC). ST and VWC are monitored at the same depths of 5, 10, 20, 40, 60, 80, 120, 160, 180, 200, 220, and 240 cm below the ground surface.

Gaps in the ST and VWC records occur from 23 January to 4 April 2025 and from 13 August to 8 November 2025. During these periods, missing ST values at 5 cm were filled using regression-based estimates derived from a separate temperature record obtained with a sensor temporarily installed at the same depth. At 240 cm depth, ST and VWC observations are sparse from 18 May to 25 November 2023. Although daily values are available, some are based on very few valid 10-minute observations. Despite the relatively small diurnal

variations in temperature and moisture at this depth, sparse sampling may still introduce bias into the daily means.

• **Better integration of the second site:** The title mentions one supersite and the start of Section 2 (l.103) focuses on the main monitoring station (SLC03). However, measurements have been acquired at a second site (SLC07) and are used in the analysis. Although it is clear that SLC07 is less instrumented, it would be easier to follow if the second station is better introduced from the start. Station SLC07 is first visible in Fig.1 but first mentioned in the text at l.137. InSAR that can be processed at the regional scale has been processed only around SLC03 (Fig.3). Why? It could have been a fine way to further discuss the differences between the two sites. To discuss the differences between the two sites, information about the surface conditions is mentioned, but not much else. What about the sediment type, the expected ice content, the climate?

Thank you very much for this valuable suggestion. We have made the following revisions to better integrate SLC07 into the analysis:

1) In **Section 2 Study area and measurement sites**, we now introduce SLC03 and SLC07 together. We have added descriptions of the surface vegetation at both sites, sediment information from the SLC03 and SLC07 borehole logs, and volumetric water content measurements.

2) In **Section 4.1.1 Ground surface deformation from Sentinel-1 InSAR**, we have extended the deformation map to include the area around SLC07, using the same spatial extent as Figure 1d to facilitate interpretation of the spatial patterns. The previous map focused on SLC03 and its surroundings to show local deformation in greater detail. We have also discussed the differences between the areas surrounding SLC03 and SLC07 in this section. The revised Section 4.1.1 is as follows:

The InSAR-derived deformation results provide a regional-scale context for interpreting the point-scale ground observations. The InSAR-derived deformation time series is fitted with a model combining a linear trend and an annual sinusoidal term to estimate the multiannual trend and seasonal deformation. The spatial patterns of the multiannual deformation trend and seasonal deformation in Figure 3a–b, viewed alongside Figure 1d, show markedly weaker deformation in the non-permafrost floodplain and on small hills than in the alpine swamp meadow and alpine meadow areas underlain by permafrost. SLC03 is situated in alpine swamp meadow, and its surroundings exhibit both large seasonal deformation and a pronounced long-term subsidence trend. In contrast, SLC07 is located near a mountain margin in degraded alpine meadow with sparse vegetation and thin soil cover. Seasonal deformation around SLC07 is markedly smaller than that around SLC03.

Figure 3c–d shows the Sentinel-1 InSAR-derived deformation time series at SLC03 and SLC07 from August 2017 to November 2025. The time series exhibits a clear seasonal cycle superimposed on a persistent long-term subsidence trend. Each year is characterized by winter freeze uplift and summer thaw subsidence, with seasonal deformation magnitude generally on the order of several centimetres. The smoothed vertical InSAR time series are divided into two intervals of approximately 4 years each, with 25 September 2021 as the temporal midpoint. At SLC03, the deformation rate changes from approximately −13.65 mm yr^{-1} during the earlier interval to −18.95 mm yr^{-1} during the later interval. At SLC07, the corresponding rates are −11.68 and −16.49 mm yr^{-1}, respectively. Compared with the earlier interval, subsidence rates in the later interval are approximately 39 % higher at SLC03 and 41 % higher at SLC07, indicating more rapid surface lowering during the more recent monitoring period. The modelled seasonal deformation increases from 51.38 to 58.12 mm at SLC03 and from 24.51 to 30.95 mm at SLC07, corresponding to increases of approximately 13.1 % and 26.3 %, respectively.

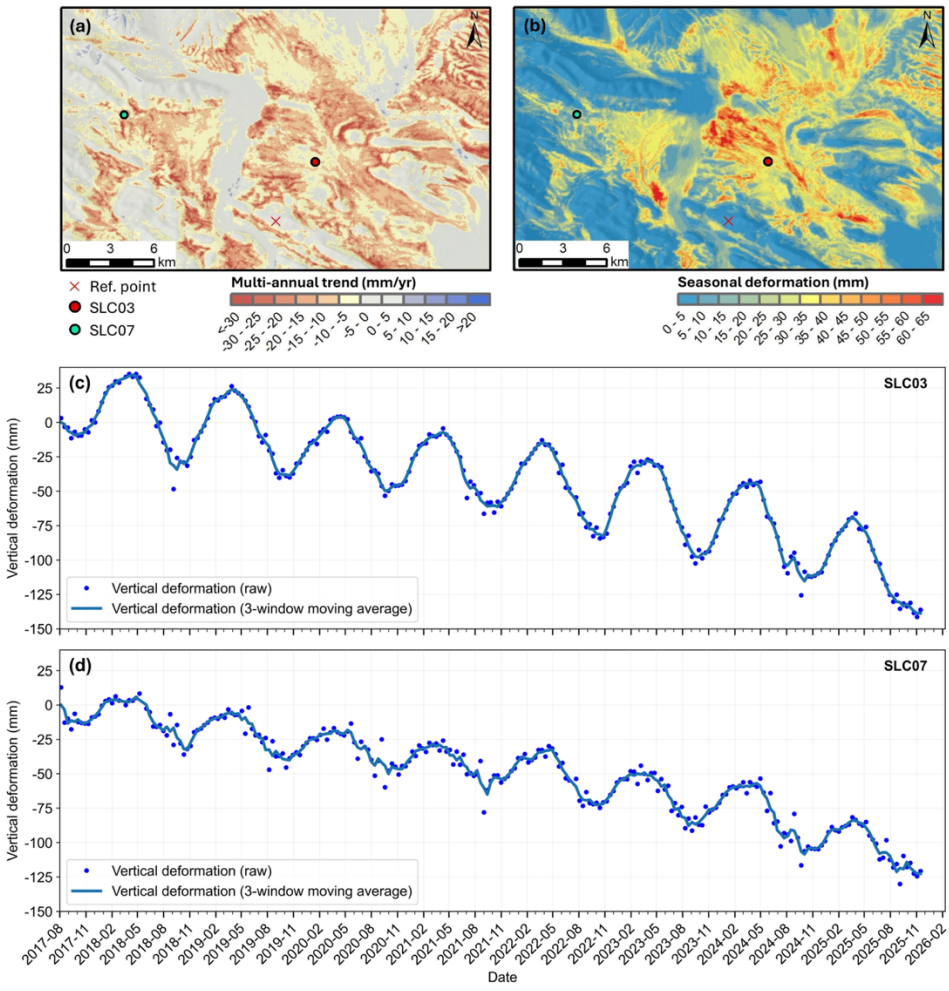


Figure 3. Sentinel-1 InSAR-derived deformation. Spatial distributions of (a) the long-term deformation trend and (b) seasonal deformation (peak-to-peak) in the radar line-of-sight (LOS) direction, shown over a hillshade basemap. (c–d) Vertical deformation time series at SLC03 and SLC07, respectively.

3) In **Section 4.2 Intercomparison of multi-sensor ground surface deformation records**, we have added a comparison involving the SLC07 LVDT observations. The comparison is presented in a supplementary figure in the appendix. The added text is as follows:

A separate comparison at SLC07 yields an InSAR-LVDT correlation of 0.71, an RMSE of 20.0 mm, and a bias of −14.5 mm (Figure A4). During the 2023–2024 freeze–thaw cycle, the LVDT record shows a marked increase in seasonal deformation range, whereas the InSAR record does not exhibit a similarly pronounced change. Agreement is particularly close over the 31 paired SAR acquisition dates from 12 November 2021 to 19 November 2022, with r = 0.98, an RMSE of 7.06 mm, and an MAE of 6.33 mm.

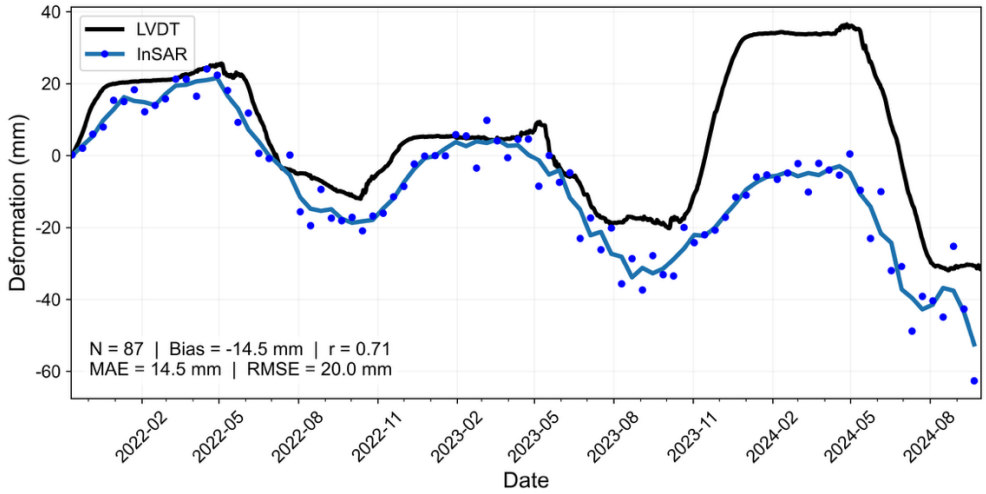


Figure A4. Comparison of LVDT and Sentinel-1 InSAR vertical deformation time series at SLC07. The black line shows the LVDT record, blue dots represent individual InSAR observations, and the blue line shows the smoothed InSAR series. Summary statistics are calculated from 87 paired observations, with bias defined as InSAR minus LVDT.

4) In **Section 5.3 Controls on the spatiotemporal variability of ground surface deformation**, we have discussed the differences between SLC03 and SLC07 and the reasons for the larger deformation at SLC07 during the 2023–2024 freeze–thaw cycle compared with the preceding two cycles. The added text is as follows:

Ground surface deformation varied substantially between sites and among years. Although only 11 km apart, SLC03 and SLC07 exhibited marked differences in seasonal deformation amplitude and the onset of thaw

settlement and freeze-back heave (Figure 4). The LVDT records from the two sites had a correlation coefficient of 0.61 and an RMSE of 29.98 mm. Interannual variability was also substantial at each site. At SLC07, both frost heave and thaw subsidence were substantially greater following higher precipitation in 2023 and a possible local increase in soil water content, resulting in a much larger seasonal deformation amplitude during the 2023–2024 freeze–thaw cycle in LVDT record (Figure 4, Appendix Figure A4). In contrast, the InSAR-derived seasonal deformation over an approximately 30 m footprint differed little between the 2023–2024 cycle and other years. These contrasting observations highlight pronounced spatial heterogeneity in ground surface deformation.

• **Improvements of table/figure contents, legends and captions:** Most figures could be slightly improved to make it easier to read. It is sometimes necessary to dig into the text to find information necessary to understand. They are often not self-contained and standalone.

Thank you for these suggestions on improving the figures and tables. We have systematically revised their legends and captions to make them self-contained and easier to read. The specific revisions addressing each comment are described below.

Some examples thereafter:

• Figure 1: Explain that panels b and c are at SLC03. c) what is the red dashed rectangle? The acronym SR50 in panel b) is not understandable (explained only at.175). Consider adding explanations of all acronyms in the caption.

Thank you for this suggestion. We have revised the SR50 label in panel b and updated the caption as follows:

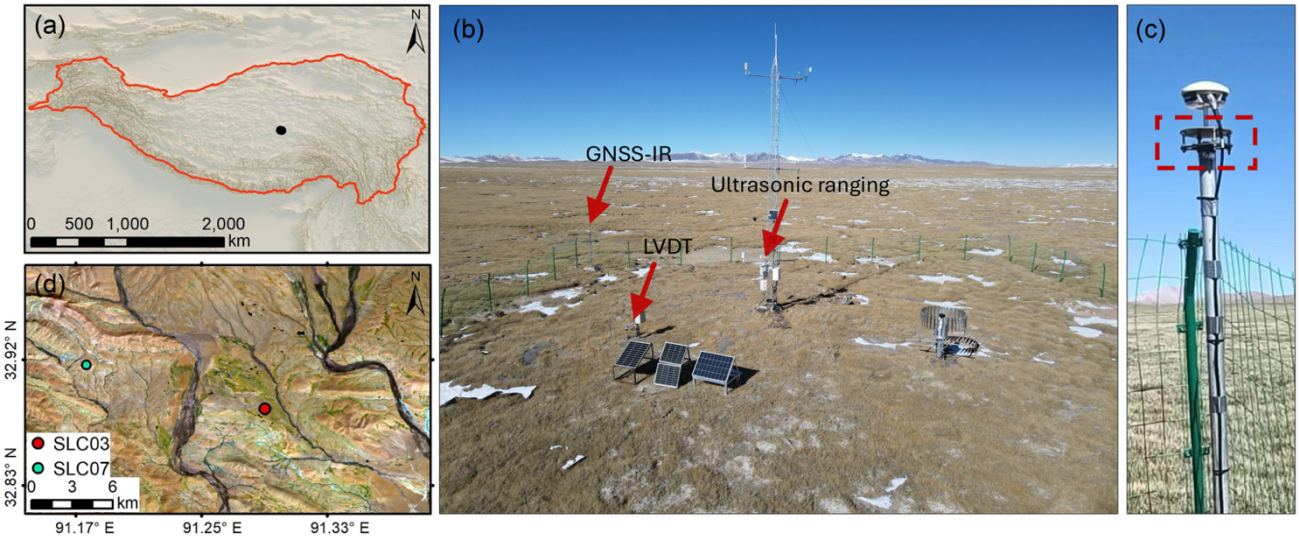


Figure 1. Study area and measurements. (a) Location of the study area on the Tibetan Plateau. (b) Instrument layout at the meteorological and permafrost monitoring station of SLC03, showing the three ground-based deformation monitoring systems (GNSS-IR, ultrasonic ranging, and LVDT) and the surrounding alpine swamp meadow. (c) GNSS antenna and its supporting structure at SLC03. The red rectangle highlights the levelling mount used to keep the GNSS antenna level. (d) Locations of the two automated LVDT-based in situ ground surface deformation monitoring sites.

• Table 1: Why not including the similar info for InSAR? Even if not an in-situ technique, the same properties could be documented and help explain the differences.

We have added InSAR information to Table 1. The revised table is provided below.

Table 1. Information on in-situ LVDT-based, ultrasonic ranging, GNSS-IR and Sentinel-1 InSAR monitoring of ground deformation.

Observation	**Observation footprint (diameter)**	**Observation interval**	**Time step used for analysis**
LVDT-based measurement	8 cm	5 min	5 min and 1 d
Ultrasonic ranging	~1 m	10 min	1 d
GNSS-IR	~50 m	1 s	1 d
Sentinel-1 SBAS-InSAR	~30 m (10 × 2 multilooking, incidence angle of 43.13°)	12 days for Sentinel-1 SAR acquisitions, with occasional 24-day intervals	12 d (occasionally 24 d)

• Figure 3: Caption: 'Spatial distribution of long-term deformation trend (a) and seasonal deformation (b)'

Following the reviewer's suggestion, we have revised the Figure 3 caption and redrawn the spatial distribution maps in panels (a) and (b) to match the spatial extent of Figure 1d, facilitating comparison with the landscape. Figure 3 now also includes SLC07.

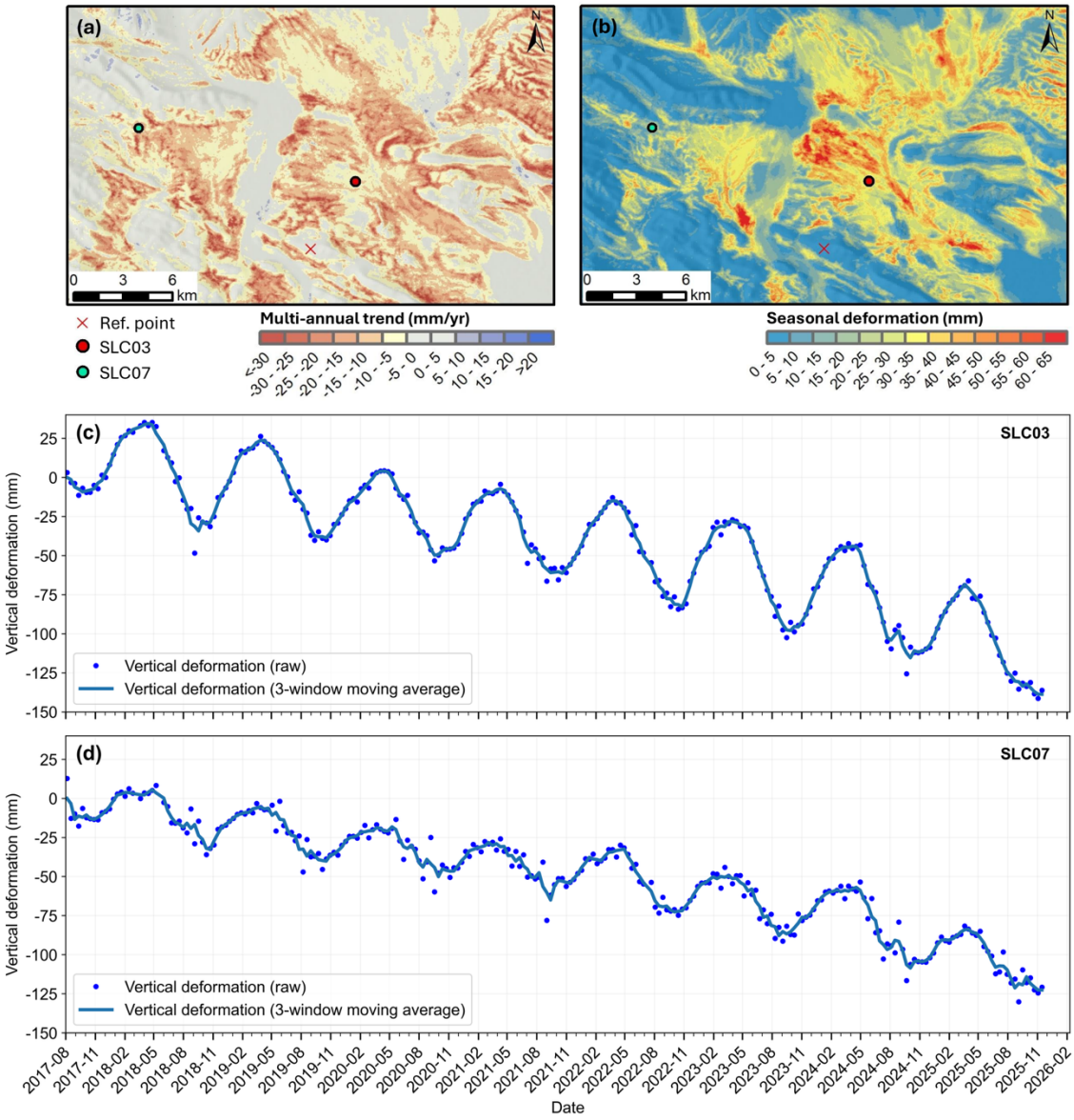


Figure 3. Sentinel-1 InSAR-derived deformation. Spatial distributions of (a) the long-term deformation trend and (b) seasonal deformation (peak-to-peak) in the radar line-of-sight (LOS) direction, shown over a hillshade basemap. (c–d) Vertical deformation time series at SLC03 and SLC07, respectively.

• Figure 4: Why is the SLC07 series stopping in summer 2024? If this is due to power-supply failures mentioned at l.289? I think it should be mentioned clearly before (methods section), because it is more than just a small data gap.

We thank the reviewer for pointing this out. The SLC07 LVDT record contains no observations after 29 September 2024 because a broken cable prevented further data acquisition. We have added this explanation to the caption of Figure 4 as follows:

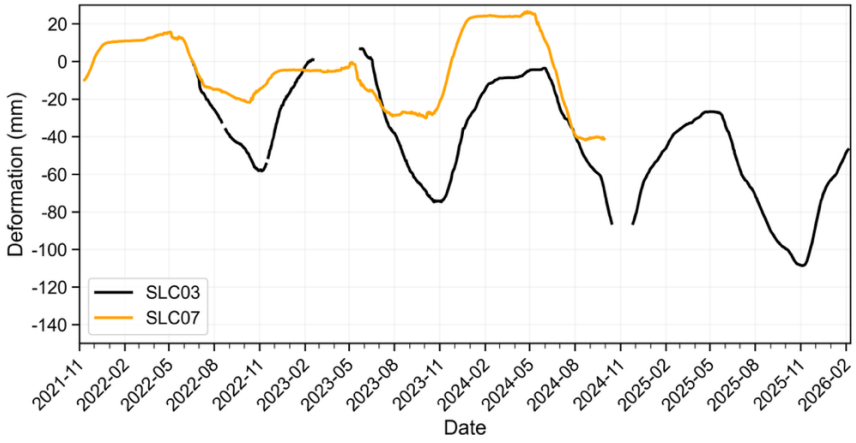


Figure 4. Multi-year ground surface deformation time series from in situ LVDT-based measurements at SLC03 and SLC07. Data gaps in SLC03 records during several periods were primarily caused by power-supply failures. In late October 2024, the LVDT record was further interrupted because ground subsidence exceeded the sensor's measurement range. Measurements resumed in December 2024, when frost heave raised the ground surface back within the sensor's measurement range. The SLC07 LVDT record ended on 29 September 2024 due to a broken cable.

• Figure 5: Orange (flag) = flagged and removed before averaging, right? Could be written more clearly in the legend or caption. The cause of the data gaps is not explained.

We have added this information to the caption. The quality control and processing of raw data are provided in the Method 3.2 Ultrasonic ranging measurements as follows:

To suppress sporadic upward spikes associated with snow or vegetation while preserving the slowly varying ground deformation signal, we applied a despiking and smoothing procedure to the daily ultrasonic ranging time series. First, a centered 7 d rolling median was used to define the local baseline, and local variability was quantified using a rolling median absolute deviation (MAD). The local MAD was scaled by a factor of 1.4826, and observations exceeding the local median by more than three times this scaled MAD (data-median>K·1.4826·MAD, with K=3) were flagged as outliers and removed. The record from 1 June 2022 to 29 November 2025 spanned 1278 days, with observations available on 1096 days and missing on 182 days. Of the available daily observations, 73 (6.66%) were flagged as outliers and removed. Internal gaps in the despiked series were temporarily filled by linear interpolation in time. The interpolated series was then smoothed using a centered 5 d median filter followed by a centered 11 d moving-average filter. Finally, the

original missing-data mask was reapplied so that dates without observations in the original record remained missing in the smoothed output.

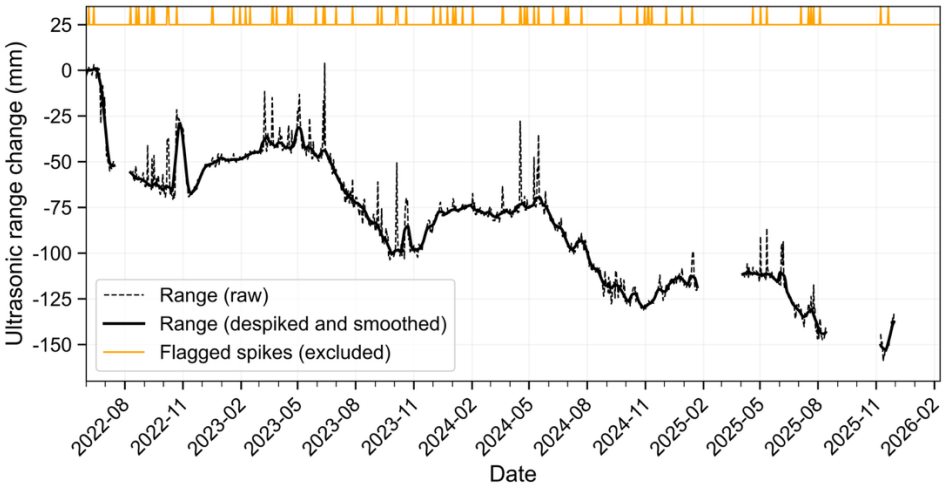


Figure 5. Raw and processed ultrasonic ranging measurements. The dotted black line shows the raw observations, and the solid black line shows the despiked and smoothed series. Orange tick marks at the top indicate the timing of observations flagged as short-lived upward spikes, mainly associated with snow. Data gaps resulted from missing records in the datalogger.

• Table 2: The names of the stages do not correspond to the naming used in Fig.10 (AT1, LT1, etc). LF stages are referred to as 2022-23, 2023-24, 2024-25, although the dates only span one year (2023, 2024, 2025). Remove or explain why AF-2025-26 is lacking information.

Thank you for this suggestion. We have redrawn Fig. 10 so that the stage names on the x-axis match those in Table 2. The AF-2025–26 entry in Table 2 now explains why the information is incomplete: the record ends on 5 February 2026. We have retained the LF stage labels LF2022-23, LF2023-24, and LF2024-25. Although these stages span February–May in 2023, 2024, and 2025, respectively, the labels match the corresponding AF stages (AF2022-23, AF2023-24, and AF2024-25) and indicate the late part of each freezing season.

Table 2. Definitions and characteristics of different freeze–thaw stages.

Freeze/thaw stage	**Criteria for identifying different freeze–thaw stages**	**Period**			**Thermal accumulation (°C·d)**
		Stage	**Date**	**Duration (days)**	
Active layer thawing (AT)	This period begins when the daily mean air temperature remains above 0 °C for seven consecutive days.	AT-2022	20220524–20220812	81	493.2
		AT-2023	20230528–20230921	117	557.3
		AT-2024	20240519–20240908	113	637.8

		AT-2025	20250524–20250820	89	482.6
Late-summer thawing (LT)	Following AT, LT represents thawing of soil layers below 220 cm and is identified by a sharp increase in soil moisture at 220 cm.	LT-2022	20220813–20221012	61	222.1
		LT-2023	20230922–20231010	19	30.7
		LT-2024	20240909–20241010	32	114.5
		LT-2025	20250821–20251010	51	180.3
Active layer freezing (AF)	This period begins when the daily mean air temperature remains below 0 °C for seven consecutive days.	AF-2022–23	20221013–20230208	119	-1498.6
		AF-2023–24	20231011–20240205	118	-1591.7
		AF-2024–25	20241011–20250215	128	-1484.1
		AF-2025–26	20251011–	End date undetermined due to missing subsequent observations; −1532.0 as of 15 February 2026.	
Late-winter freezing (LF)	Following AF, LF is identified when soil liquid water content at 220 cm shows a sharp decrease and falls below 0.1 m^3/m^3.	LF-2022–23	20230209–20230527	108	-811.0
		LF-2023–24	20240206–20240518	103	-842.7
		LF-2024–25	20250216–20250523	97	-627.8

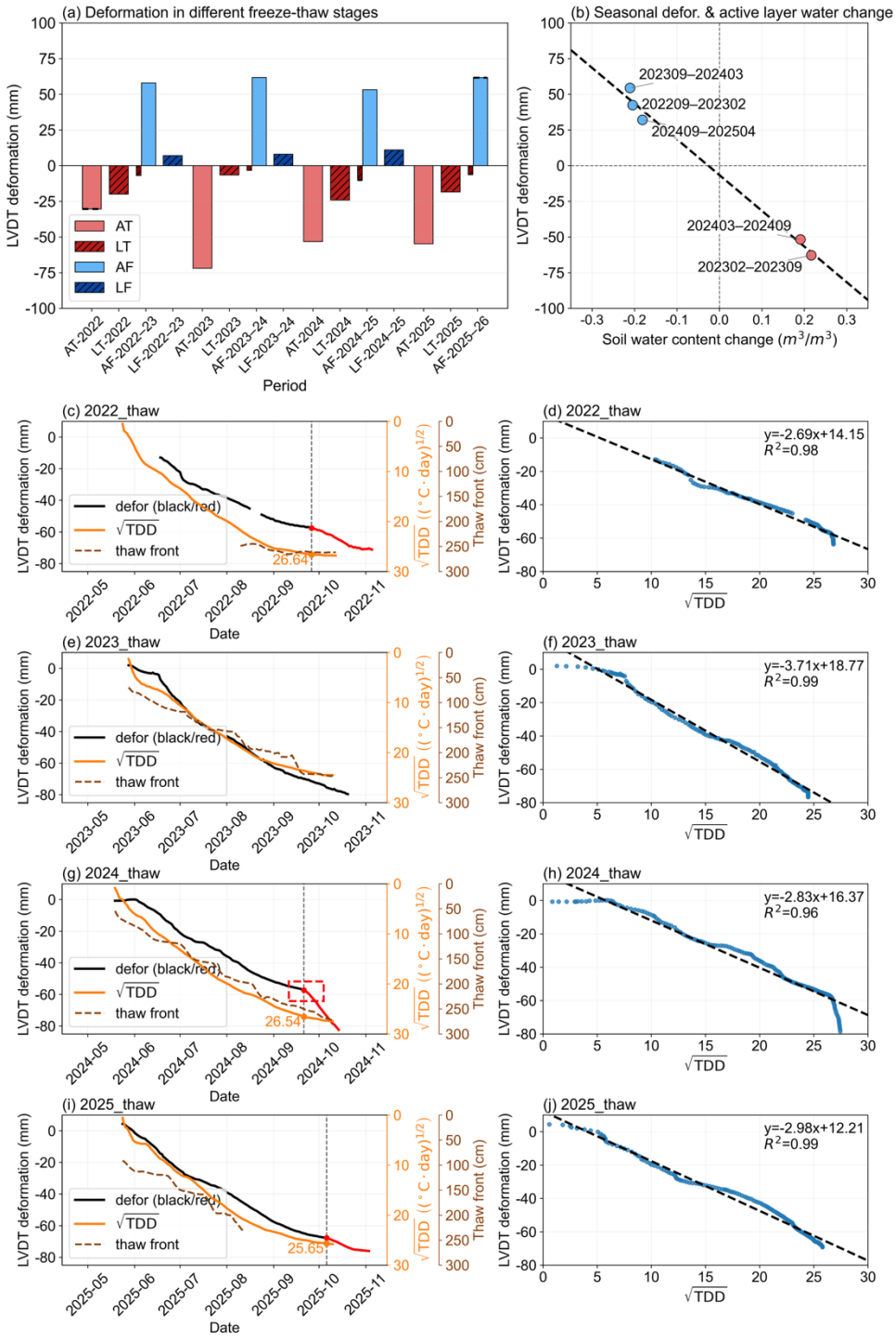


Figure 10. Deformation characteristics across freeze-thaw stages and their relationships with thaw progression. (a) Deformation partitioned into active thaw (AT), late thaw (LT), active freezing (AF), and late freezing (LF) stages for different annual cycles. (b) Seasonal deformation and active layer water content change. (c, e, g, i) Deformation curves, √TDD, and thaw-front depth during the thaw seasons of 2022, 2023, 2024, and 2025. For ease of intercomparison, the deformation time series was shifted such that the deformation was approximately zero at √TDD = 5. Black and red segments indicate deformation before and after the late-season breakpoint, respectively. Orange numbers at the base of the orange lines in (c), (g), and (i) indicate the √TDD values corresponding to the deformation breakpoints. No breakpoint was detected in

2023 (e), the coldest of the four years. (d, f, h, j) Relationships between thaw-season deformation and √TDD for the corresponding years, together with linear regressions.

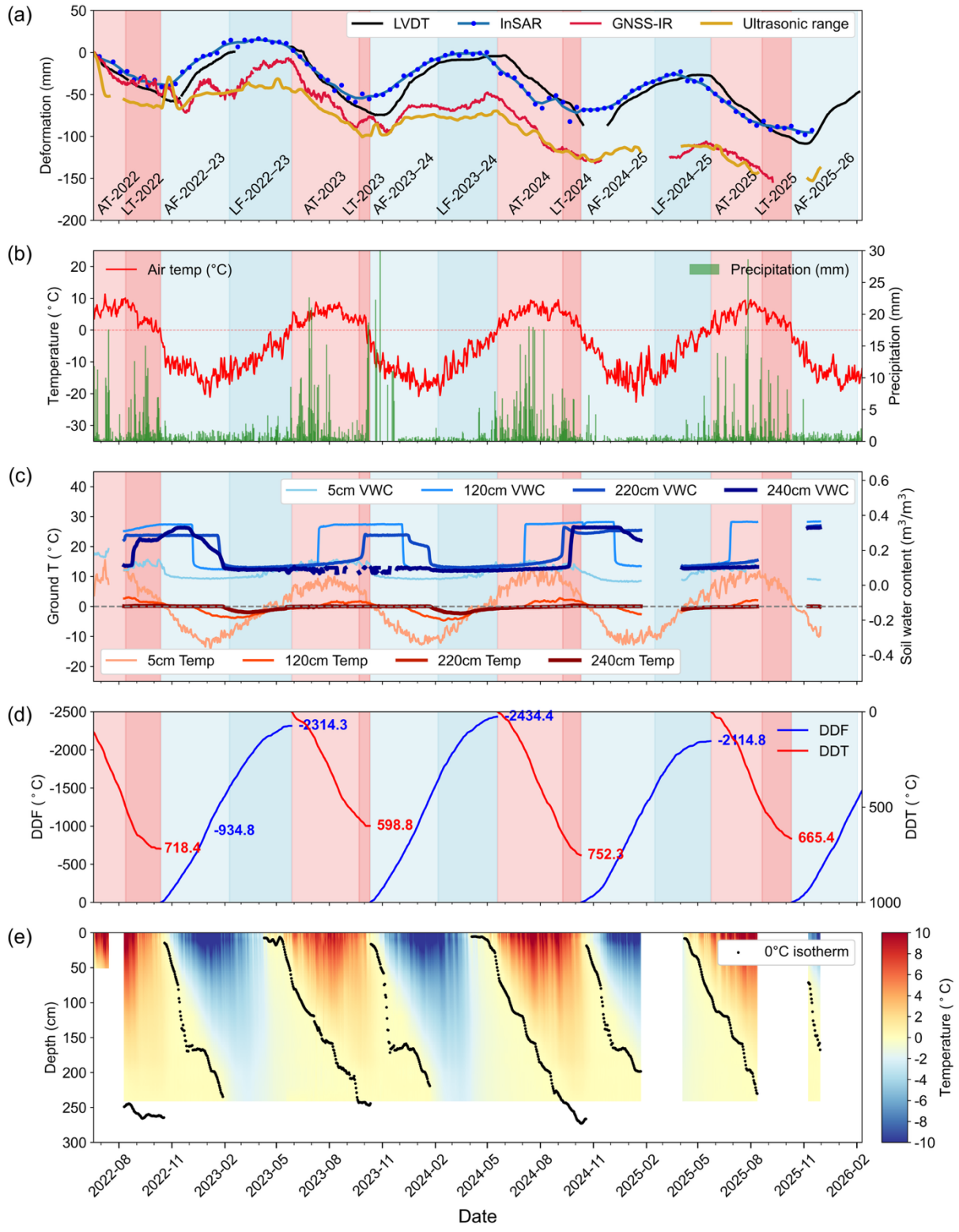
• Figure 7: In (a), none of the displacement time series start at zero. L.338 explains that the series are referenced to the first day. Which first day? Different for each technique? If yes, for sake of comparison in this graph, why not referencing everything to June 2022? The legend of the stages (AT, LT, AF, LF) could be added to the figure for better standalone understanding. The acronym could be explained in the caption. It might be a color contrast question, but it seems that the black line (thaw front) in (e) does not match 0 degree and therefore it is unclear how this line has been plotted.

Thank you for this suggestion. We have redrawn Figure 7 and referenced all deformation records to 18 June 2022. We have also added a legend for the freeze–thaw stages (AT, LT, AF, and LF) and explained the abbreviations in the caption.

The plotted 0 °C isotherm depths were estimated from daily soil temperature profiles using vertical interpolation and, where applicable, extrapolation. We have added a detailed description of the calculation to Section 3.5 and now display the estimates as points in panel (e). We have also adjusted the y-axis in panel (e) to show the estimated maximum thaw depth for each year more clearly. The apparent discrepancy within the 120–160 cm depth interval may reflect the absence of temperature measurements at 140 cm and the small temperature differences between depths during the freezing season.

The added statements are as follows:

“Daily 0 °C isotherm depths are estimated from daily soil temperature profiles. Zero-valued temperatures are excluded from the crossing search, and the crossing depth between adjacent valid, nonzero temperatures of opposite signs is calculated by linear interpolation. Extrapolation is attempted only when all valid profile temperatures are strictly positive and measurements at 200, 220, and 240 cm are available. In these cases, an ordinary least-squares linear regression of temperature against depth is fitted to these three measurements, and the fitted line is extrapolated to 0 °C. The resulting depth series is processed separately within each thawing and freezing segment. Internal gaps are filled by linear interpolation in time, followed by smoothing with a centered 7 d moving average that includes the current day and up to three days on either side. Averaging windows are truncated at segment boundaries and use only available values.”



Multi-sensor ground surface deformation and hydrothermal conditions at the SLC03 supersite during 2022–2026. (a) Ground surface deformation time series derived from LVDT, Sentinel-1 SBAS-InSAR, GNSS-IR, and ultrasonic ranging. The deformation time series from different observation methods were referenced to 18 June 2022. Shaded blue and red bands indicate freezing and thawing stages, respectively. Light red and red represent Active layer thawing (AT) and Late-summer thawing (LT), and light blue and blue represent Active layer freezing (AF) and Late-winter freezing (LF). (b) Daily air temperature and precipitation. (c) Soil

temperature and volumetric water content at 5, 120, 220 and 240 cm depth. (d) degree days of thawing (DDT) and degree days of freezing (DDF). (e) Soil temperature profile; the black dot indicates the estimated 0 °C isotherm based on soil temperature profile.

• Figure 9: References to the different freeze-thaw stage names could be added in the figure to help the readers.

Thank you for this suggestion. The freeze–thaw stage names are now labelled directly in the figure.

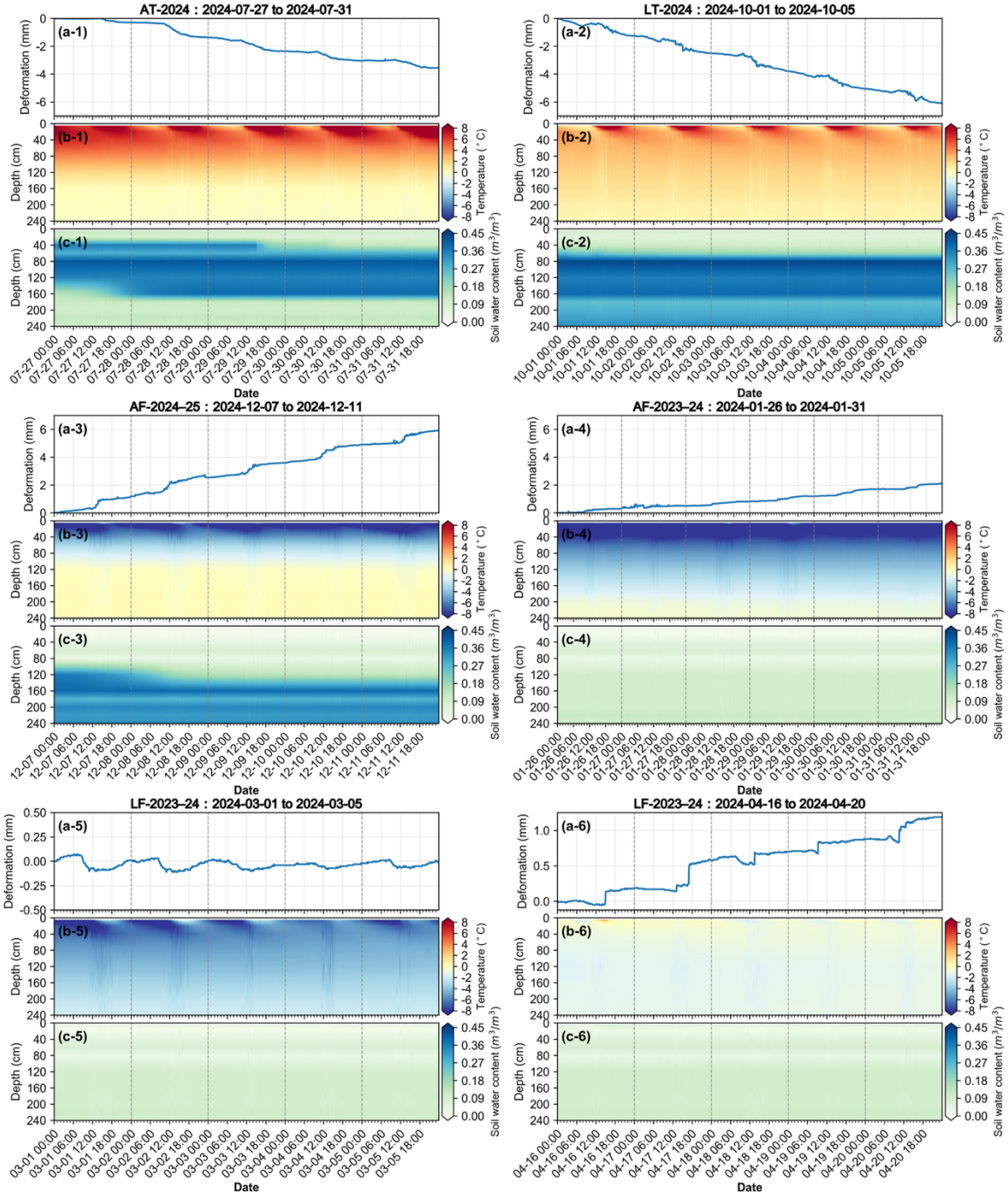


Figure 9. Representative sub-daily ground surface deformation, together with the corresponding soil temperature and moisture profiles, during different freeze–thaw stages. Panels a present ground surface

deformation at 5 min resolution, with the time series shifted so that the value at the first time step is zero. Panels b and c show soil temperature and soil moisture profiles, respectively, at 10 min resolution.

• Figure 11: Add a reference to Fig. 10g (full series).

Thank you for this suggestion. We have added a dashed box to Figure 10g to mark the period shown in Figure 11. The Figure 11 caption now also includes a reference to the full time series in Figure 10g.

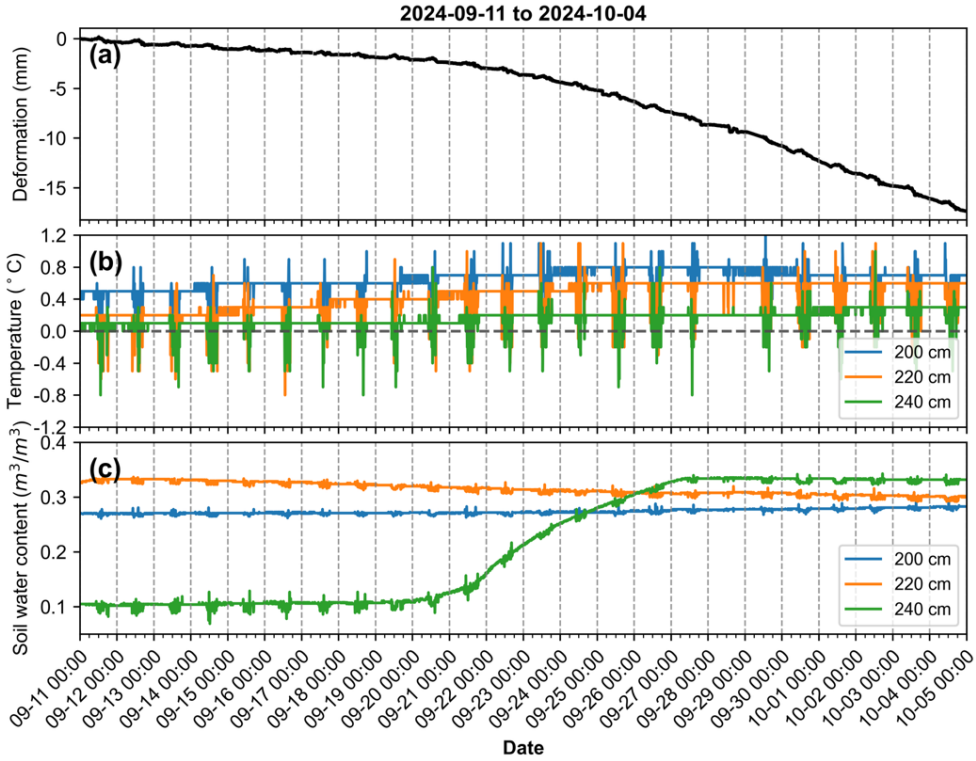


Figure 11. Late-thaw-season accelerated subsidence and associated hydrothermal profiles at the base of the active layer (200–240 cm) during 20240911–20241004. This interval is highlighted by a red dashed box in the full time series for the 2024 thaw season (Figure 10g). (a) Ground surface deformation recorded by the LVDT sensor at 5 min intervals. The deformation time series was shifted such that the value at the first time step was set to zero. (b, c) Soil temperature and moisture time series at 10 min intervals.

• Figure A3: Somewhat at the same level as Fig. 11 (short-term analysis) and very much supporting what is described in Section 4.4.3. It would make sense to move it to the main manuscript.

Thank you for this suggestion. We have moved Figure A3 to Section 4.4.3 of the main manuscript, where it is now Figure 12. We have also refined the figure and extended the analysis period to better explain this process. The revised figure and accompanying text are provided below:

4.4.3 Late-freezing slight heave and refreezing of infiltrated water

Small but distinct heave events are observed at both sites between mid-April and early May, including at SLC03 in 2024 and 2025 and at SLC07 in 2022–2024 (Figure 4). Figure 9a-6 illustrates the detailed deformation time series during 16–20 April 2024 at SLC03. The deformation progresses through discrete, rapid upward steps separated by short plateaus, contrasting with the smoother winter uplift observed during other periods (e.g., Figure 9a-3 and a-4).

Figure 12 extends this analysis to 30 April 2024, combining the deformation record with soil temperature and moisture observations in the upper 20 cm and ultrasonic snow depth estimates. Five upward steps are identified in Figure 12a: 0.18 mm at approximately 15:00 on 16 April, 0.30 mm at approximately 17:00 on 17 April, 0.32 mm at approximately 08:20 on 22 April, 0.44 mm at approximately 17:15 on 25 April, and 0.22 mm at approximately 10:40 on 29 April. Four of these five steps occur on the same day as, or the day after, snow depth increases recorded by ultrasonic ranging (Figure 12b). Snow depth increases relative to the preceding day by 6.82 mm, 42.90 mm, 3.53 mm, and 5.51 mm on 16, 17, 24, and 28 April, respectively. Snow accumulation on these days is followed by decreases in snow depth, consistent with subsequent snowmelt. The heave events also coincide with, or follow, shallow soil warming and increases in soil moisture. Daily maximum temperatures at 5 cm reach 3.7 °C on 16 April and 3.8 °C on 24 April. Volumetric water content at 5 cm is elevated around these events compared with values on nearby dates, with daily maxima reaching approximately 0.09 m^3/m^3 on 16 April and 0.10–0.13 m^3/m^3 on 21–22, and 24–25 April. During some heave events, however, diurnal soil temperature fluctuations are suppressed. On 17 April, temperature variations at 5 cm are damped, with a daily minimum of −1.1 °C and a maximum of 0.0 °C; the temperature remains nearly constant at approximately −0.1 °C from 18:00 to 22:00, rather than exhibiting the usual diurnal oscillation. Temperature fluctuations on 25 April are also smaller than on the preceding days. Such temperature stabilization near the freezing point may reflect latent heat released during refreezing. Together, the snow depth changes, elevated shallow soil moisture, suppressed temperature fluctuations, and stepwise heave support the interpretation of snowmelt infiltration followed by rapid refreezing in the shallow soil.

A similar feature is observed at SLC07 in April 2022, where slight heave is followed by brief subsidence and then renewed slight heave before the onset of sustained thaw settlement. This “shallow trough” in the late-

winter deformation record may likewise reflect alternating thawing and refreezing associated with infiltrated water.

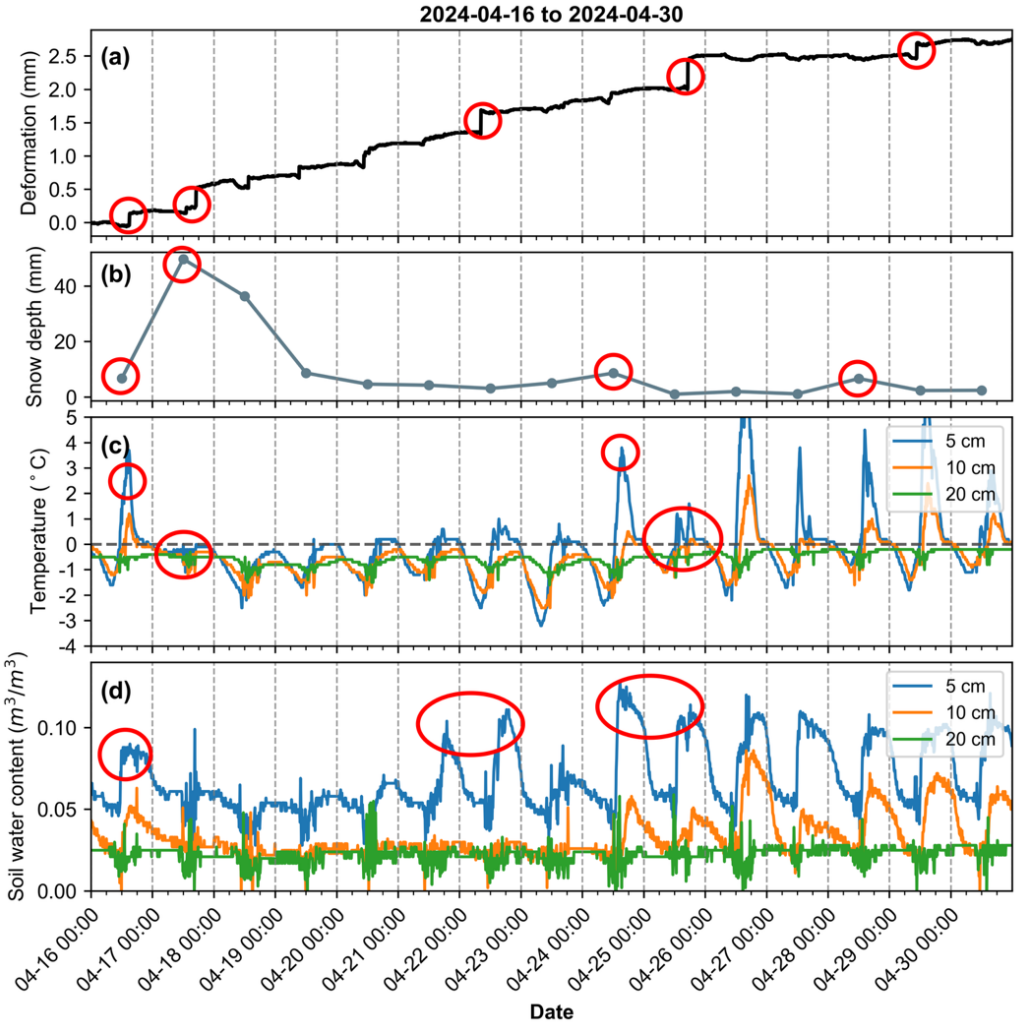


Figure 12. Sub-daily ground surface deformation and concurrent soil temperature and moisture profiles at 5–20 cm depth during 16–30 April 2024. Snow depth was derived from daily raw ultrasonic ranging data and is presented relative to 15 April 2024.

• Figure 10: A lot of information in this figure. Ensure that all elements are well explained. For ex. what is the orange number at the bottom of the TDD dashed lines in c, e, i? And why missing in g? It could be mentioned in the caption that the displacement time series are based on LVDT only.

We have clarified in the caption that the orange numbers at the base of the vertical dashed lines in panels (c), (g), and (i) indicate the $\sqrt{\text{TDD}}$ values corresponding to the deformation breakpoints. No number is shown in panel (e) because no breakpoint was detected in 2023, the coldest of the four years. The deformation axes are labelled "LVDT deformation" to make clear that the displacement time series are based solely on LVDT observations. We have also adjusted the axis colors to distinguish $\sqrt{\text{TDD}}$ from thaw-front depth more clearly.

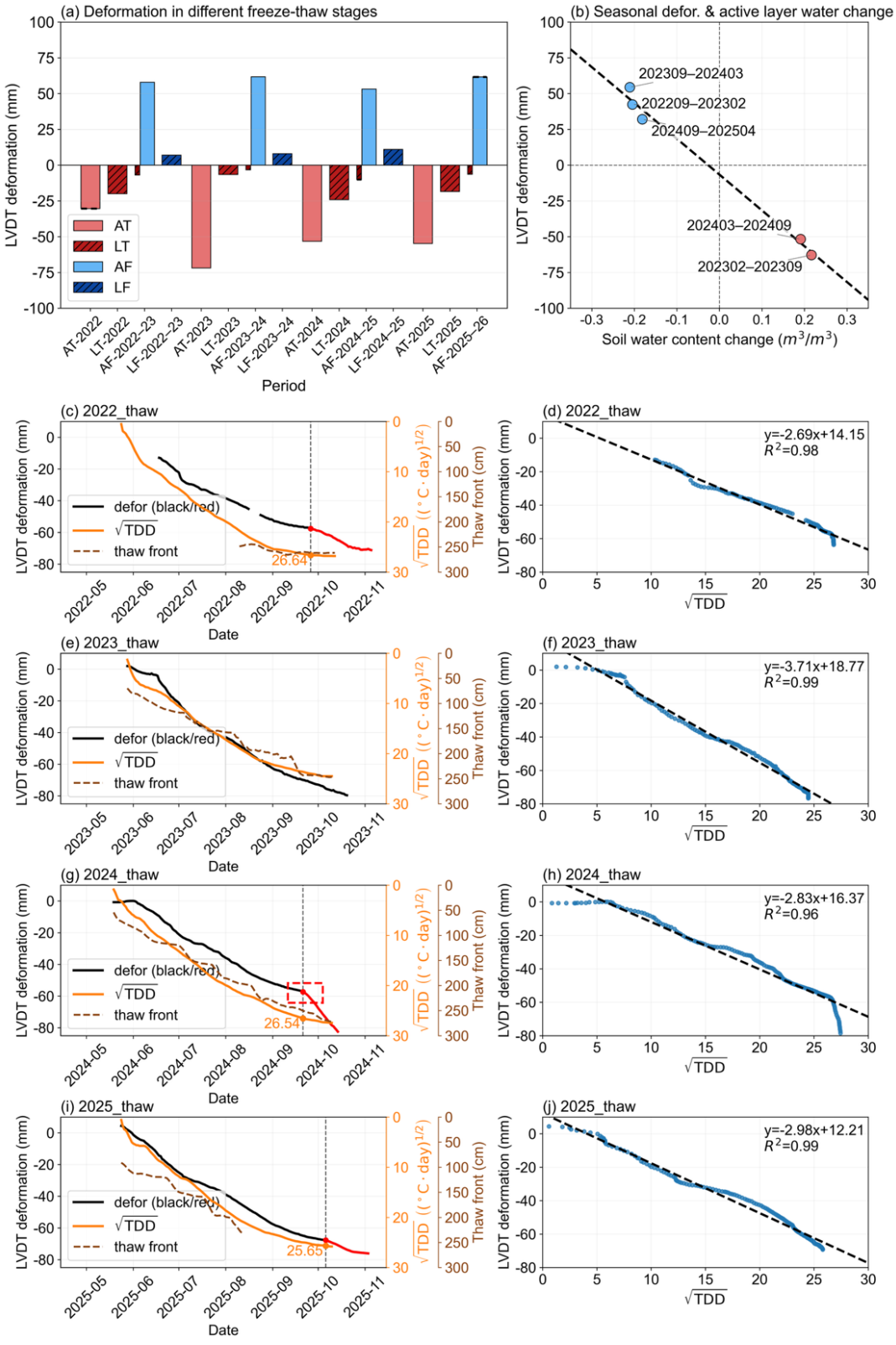


Figure 10. Deformation characteristics across freeze-thaw stages and their relationships with thaw progression. (a) Deformation partitioned into active thaw (AT), late thaw (LT), active freezing (AF), and late freezing (LF) stages for different annual cycles. (b) Seasonal deformation and active layer water content change. (c, e, g, i) Deformation curves, $\sqrt{\text{TDD}}$, and thaw-front depth during the thaw seasons of 2022, 2023, 2024, and 2025. For ease of intercomparison, the deformation time series was shifted such that the

deformation was approximately zero at $\sqrt{\text{TDD}} = 5$. Black and red segments indicate deformation before and after the late-season breakpoint, respectively. Orange numbers at the base of the orange lines in (c), (g), and (i) indicate the √TDD values corresponding to the deformation breakpoints. No breakpoint was detected in 2023 (e), the coldest of the four years. (d, f, h, j) Relationships between thaw-season deformation and $\sqrt{\text{TDD}}$ for the corresponding years, together with linear regressions.

• **Discussion of the AL vs top-of-permafrost ice melt, and the pore ice vs excess ice controls:** A major point of the article is to discuss the differences of displacement patterns from ground thawing during the main spring-summer period (melt of ice in the active layer) and during the late-thaw-season (melt of ice at the top of the permafrost). Of course, the records are very interesting due to the high temporal resolution, and I overall agree with the interpretation, but the explanations are not always clear. The point is discussed several times (l.23-26; l.81-82; l.479-506; l.635-647) but remains at the same level along the paper, and somewhat mixes the question of the temporality (early/mid-season vs late-season) and the type of ice (pore ice vs excess ice) and the depth of the thaw front (AL, top-of-permafrost) without providing all information to make the links between these elements. At several locations, it seems to assume that excess ice is only in the deepest layers, at the top of the permafrost (section 4.4.2, l.591, l.639). Subsidence from active layer thaw is also due to ice melting and can also include a component from excess ice. That is shown in some references you are included at l.82-84you're your case, how do we know that the active layer has no excess ice? How do we know that the late-season subsidence corresponds to a thaw front reaching the top of the permafrost, considering that the ALT is estimated at 300 cm (l.118) but that the temperature sensors are not measuring below 240 cm (l.235). L.669 -670 list several contributions: 'distinct deformation behaviours during active layer thaw, excess ground ice melt, active layer freezing, etc.' and l.670-672 mention that 'settlement during active layer thaw commonly occurred in a stepwise manner, whereas settlement by excess ground ice melting was more continuous'. Phrased this way, it sounds that movement from active layer thaw is not from ice melting. I guess you mean that it is due to pore ice melt only (by opposition to the deepest layers), but in that case, better to state it clearly. It is just a matter of phrasing and clearer explanations about the links between the thaw front depth, the ice type and content, and the resulting subsidence patterns.

Thank you for helping us clarify the different roles of pore ice and excess ice in controlling ground surface deformation. To make the explanation clearer and easier to follow, we have made the following revisions:

1) In the Study area section, we have added descriptions of borehole core observations at SLC03, together with field measurements of the soil water content (ground ice) profile at different depths, to better characterize the possible distribution of ground ice at the site. The added text is as follows:

2 Study area and measurement sites

Borehole drilling conducted during the Second Tibetan Plateau Scientific Expedition in November 2019 provided the foundation for subsequent permafrost observations. By this time of year, seasonal thaw is generally expected to have reached its maximum depth. The 2019 field records document contrasting surface conditions at the two sites. Site SLC03 occupies a flat valley floor supporting alpine swamp meadow, with approximately 90 % vegetation cover, locally degraded frost-heave hummocks, and exposed gravel. SLC07 is situated in degraded alpine meadow with sparse vegetation, a dry, sandy surface containing gravel, and pronounced soil salinization. The boreholes reach depths of 30 m at SLC03 and 20 m at SLC07. At SLC03, the drilling log describes fine sand with gravel in the upper meter, underlain by gravelly sand between 1.0 and 4.6 m depth, tentatively interpreted as glaciofluvial deposits. Ice crystals are visible at 2.4–3.0 m, and the core recovered from 3.0–4.5 m contains abundant water and has a slurry-like consistency. Discrete ice layers occur at greater depths, including an approximately 2.5 mm thick layer within 4.6–5.1 m, a 2.8 cm thick pure-ice layer at 7.3–7.4 m, and a 30 cm thick pure-ice layer at 16.0–16.3 m. Volumetric water content in borehole core samples from SLC03 varied substantially across depths of 0.2–29.4 m, with a mean of 0.32 m^3/m^3 and particularly high values of 0.47 and 0.56 m^3/m^3 at 2.7 and 4.6 m, respectively (Appendix Figure A1). Subsequent active layer temperature and moisture profiles indicate an active layer thickness (ALT) of approximately 2.4 m. Together with the drilling records, these observations suggest the presence of excess ice near the top of permafrost. At SLC07, the drilling log describes dry sandy soil at 0–0.7 m, clay at 0.7–1.6 m, and rock at 1.6–3.5 m. Abundant liquid water was observed in the fragmented core recovered from 2.5–3.5 m. Clay containing angular rock fragments occurs at 3.5–6.0 m, where liquid water but no visible ice was recorded. Rock dominates the 6.0–18.0 m interval, with liquid water noted at 6.0–6.5 m, whereas grey clay containing gravel occurs at 18.0–20.0 m, with no visible ice recorded. Volumetric water contents at depths of approximately 0.5, 1.2, and 3.5 m are 0.31, 0.42, and 0.27 m^3/m^3, respectively.

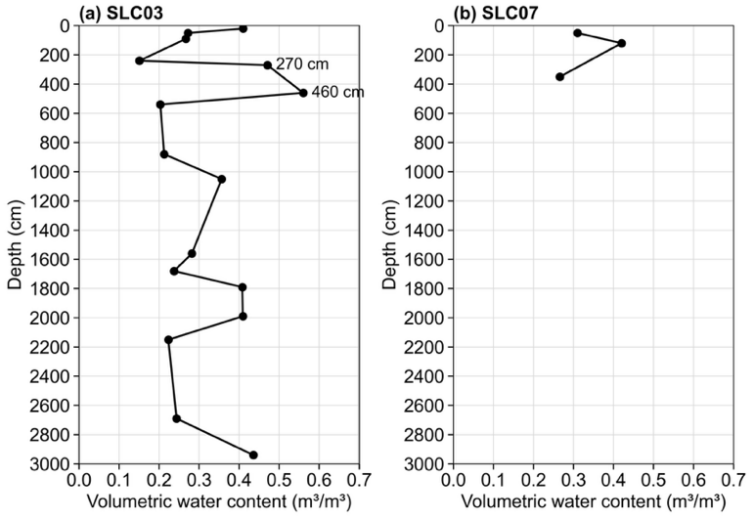


Figure A1. Volumetric water content profiles from borehole core samples collected at (a) SLC03 and (b) SLC07. Black circles denote values at sampling depths.

2) We have clarified that the previously stated ALT of approximately 3 m represents the regional average, whereas ALT at SLC03 is approximately 240 cm. Borehole-core observations provide supporting evidence and indicate the presence of excess ice below the active layer. Ice crystals were recorded at 240–300 cm during drilling on 9 November 2019, confirming that the soil was frozen. The active layer temperature and moisture profiles also suggest an ALT of approximately 240 cm. Using 20 November–10 December as the annual comparison window, mean volumetric water content at 240 cm was 0.317, 0.098, 0.331, and 0.329 m^3/m^3 in 2022, 2023, 2024, and 2025, respectively. These values suggest that thaw did not reach 240 cm in 2023. The corresponding mean soil temperatures were 0.056, 0.023, 0.068, and 0.048 °C, respectively, all close to 0 °C, suggesting that the active layer base was near 240 cm.

3) We have clarified ambiguous passages and removed the wording at lines 670–672 to avoid confusion. The relevant text in **Section 5.2 Significance of sub-daily deformation observations for process interpretation**, has been revised as follows:

A second example concerns the previously observed acceleration of subsidence during the late thaw season, which the 5-min deformation record helps explain. This record shows systematic differences between deformation associated with pore ice melt within the active layer and that associated with excess ice melt at the top of permafrost. Settlement during active layer pore ice melt is commonly stepwise, as shown in Figure 9a-1, whereas settlement after the late-season breakpoint becomes more sustained and pronounced, consistent with continued drainage and compression following excess ground ice melt.

4) We have expanded the discussion of excess ground ice in Section 5.4 Deformation-based indicators of excess ground ice melt as follows:

5.4 Deformation-based indicators of excess ground ice melt

In situ observations in Svalbard documented a late-thaw-season acceleration in subsidence associated with thaw penetration into an ice-rich layer (Harris et al., 2011). A similar breakpoint-like acceleration near the end of the thaw season is apparent in the in situ deformation records presented by Fan et al. (2025) on the Tibetan Plateau. Complementing these field observations, InSAR analyses supported by in situ measurements on the Yamal Peninsula linked enhanced subsidence during an unusually warm summer to excess ground ice melt at the base of the active layer (Bartsch et al., 2019). More recent InSAR-based work in Svalbard revealed marked differences between subsidence associated with pore ice melt and that associated with excess ice melt (Wendt et al., 2026). In Alaska, InSAR observations showed that late-season subsidence during exceptionally warm summers was much greater in ice-rich than in ice-poor terrain (Zwieback & Meyer, 2021), supporting its use as an indicator of ice-rich permafrost. Subsequent studies demonstrated the potential of InSAR-derived subsidence for estimating excess ground ice content (Zwieback et al., 2025; Zwieback, Iwahana, et al., 2024). Our observations support this interpretation and show that late-thaw-season subsidence acceleration in warm years provides a useful process-based indicator of excess ice melt at the top of permafrost. When the thaw front reaches ice-supersaturated material, excess meltwater is generated, and subsequent drainage and thaw consolidation lead to enhanced surface lowering. In contrast, thawing of ice-undersaturated or merely saturated soil produces little excess water and therefore little additional settlement. In this context, a late-thaw-season breakpoint-style acceleration in subsidence following a substantial slowdown is best interpreted as a process-specific signature of thaw front reaching the ice-rich permafrost. In our record, such acceleration is evident in year 2022 (20220926), 2024 (20240921), and 2025 (20251006), but not in 2023, a relatively cold year with the lowest TDD among the four years (Figure 7d).

The occurrence, timing, and magnitude of these breakpoints depend on heat accumulation, the vertical distribution of ground ice, and local drainage conditions, all of which can sharpen or smooth the deformation response. Although excess ice is often particularly abundant near the base of the active layer and in the uppermost permafrost (Shur et al., 2005), it can also occur elsewhere within the active layer, where its melt may likewise alter the deformation response (Wendt et al., 2026). If excess ice is scarce or the contrast in ice content

between layers is small, the acceleration signal can be weak relative to measurement noise and obscured by spatial averaging. This limitation is also illustrated at SLC03, where the LVDT record shows a clear late-thaw-season acceleration, whereas the corresponding feature is much less distinct in GNSS-IR, ultrasonic ranging, and InSAR. Under such conditions, the multiannual subsidence trend may serve as a more robust indicator of the ground ice loss. InSAR provides a means of monitoring ground surface deformation over broad areas, and this study demonstrates that Sentinel-1 SBAS-InSAR can provide reasonably accurate deformation estimates in alpine meadow environments on the Tibetan Plateau. Sentinel-1 has accumulated approximately a decade of C-band SAR observations over many permafrost regions (Bartsch et al., 2026). Complementary L-band observations from NISAR offer the potential to extend deformation monitoring to more densely vegetated terrain, where C-band observations are particularly susceptible to decorrelation. In the Arctic, however, retrieving continuous multiannual deformation time series using InSAR is often challenging because winter snow cover and wet snow during spring snowmelt can cause strong decorrelation. In such cases, thaw-season deformation curves, along with interannual comparisons of thaw-season deformation processes, may still provide valuable information on excess ice melt.

• **Comparison between the different methods and discussion of each technique value/limitations:** Four methods are used to measure ground surface displacements. All have different properties and therefore advantages and limitations. The techniques are compared using correlation metrics, but in some cases without discussing much the observed differences. More weight is placed on LVDT, which is understandable due to the high temporal resolution. However, to strengthen the clarity of the conclusions and better highlight the value of the multi-sensor supersite, I believe a more balanced treatment of the other techniques and more discussions of the differences would be valuable.

Thank you for this suggestion. We have added dedicated paragraphs to the Discussion to provide a more balanced assessment of the characteristics, advantages, and limitations of all four monitoring methods. We have discussed why LVDT and InSAR show closer agreement, as do GNSS-IR and ultrasonic ranging, and explained the differences in deformation timing between LVDT and InSAR. We have also expanded the discussion of the value and limitations of InSAR for regional observations and added an InSAR summary to the conclusions. The detailed revisions are described below.

Some examples thereafter:

• Figure 7: the InSAR and LVDT time series show a major shift of displacement patterns (several months of differences in the timing of the subsidence-heave cycle). Any idea why? It is mentioned several times in the text that InSAR and LVDT are well agreeing in term of correlation (e.g., l.362), but it is not necessarily the case temporally.

Thank you for this suggestion. We have explained this discrepancy in the manuscript and revised Figure 7 to make the differences clearer. Panel (a) now shows the raw InSAR observations as points and the smoothed results as a line. In **Section 4.2 Intercomparison of multi-sensor ground surface deformation records**, we explain this discrepancy as follows:

Despite the similarities between LVDT and InSAR in deformation patterns, multiannual trends, and seasonal deformation, differences remain in the apparent timing of freeze–thaw deformation. The native InSAR sampling interval of approximately 12 d and temporal smoothing limit the precision of onset estimates. Nevertheless, Figure 7a shows that sustained thaw settlement begins later in the LVDT record than in the InSAR record, particularly at SLC03. This discrepancy may partly reflect differences in spatial support (~30 m for InSAR versus 0.08 m for LVDT; Table 1), combined with surface heterogeneity and differences in local soil conditions. At the onset of sustained LVDT settlement at SLC03, the thaw front depths estimated by interpolating the soil temperature profiles are already 61.4 cm, 85.1 cm, and 85.8 cm on 27 May 2023, 1 June 2024, and 19 May 2025, respectively. The depth-weighted mean volumetric water content in the upper 60 cm during late May (20–31 May) is 0.085 m^3/m^3, 0.116 m^3/m^3, and 0.083 m^3/m^3 in 2023, 2024, and 2025, respectively. The two nearby soil sensor arrays (less than 10 m apart) also record contrasting shallow soil moisture conditions. During 20–31 May in 2023–2025, depth-weighted mean volumetric water content in the upper 10 cm ranges from 0.080 to 0.101 m^3/m^3 in the newer array and from 0.173 to 0.225 m^3/m^3 in the older array. These observations suggest that relatively dry shallow soil and pronounced soil moisture heterogeneity may contribute to the delayed onset of sustained settlement at the LVDT measurement point and to differences among the monitoring methods. In addition, the InSAR-derived deformation signal may be affected by snow accumulation and melt. Repeated snowfall and snowmelt during the early thaw season (Figure 5) may therefore also contribute to the earlier apparent onset of settlement in the InSAR record compared with the LVDT record.

• L.345-349 and Figure 8: Methods measuring larger seasonal amplitudes are also those showing smaller long-term trend. Any idea why?

In Section 5.1, we discuss why methods showing larger seasonal amplitudes also show smaller long-term subsidence trends. We consider frost jacking of the GNSS-IR and ultrasonic ranging benchmarks might be the most likely explanation. The LVDT reference is anchored at 30 m depth, whereas the GNSS-IR and ultrasonic ranging foundations are anchored at 6 m and might experience frost jacking. If the benchmarks move upward with the ground surface during winter, part of the actual frost heave is offset in the relative measurements, reducing the recorded heave. If the benchmarks do not fully return to their previous elevations during thaw, residual uplift makes the ground surface appear lower in the same season of the following year, exaggerating cumulative apparent subsidence. Incomplete recovery after frost jacking can therefore lead to upward benchmark movement accumulating over successive years. We have expanded the discussion of this effect in Discussion Section 5.1 Deployment and performance of the in-situ ground surface deformation monitoring system in permafrost terrain.

• L.355-356: LVDT-InSAR are more similar to each other, and GNSS-IR and ultrasonic ranging are also more similar to each other. Any idea why?

We have clarified this pattern in the results presented in Section 4.2 and expanded the discussion of ground-based monitoring benchmarks in Section 5.1 Deployment and performance of the in-situ ground surface deformation monitoring system in permafrost terrain. We explain that the similarity between GNSS-IR and ultrasonic ranging may largely reflect shared effects of frost jacking, whereas the deeper LVDT benchmark is less susceptible to this process and therefore provides a more stable reference for ground surface deformation measurements. The revised text in the main manuscript is as follows:

4.2 Intercomparison of multi-sensor ground surface deformation records

The larger subsidence trends derived from GNSS-IR and ultrasonic ranging may reflect pronounced local thaw settlement associated with installation disturbance within their observation footprints. This interpretation is consistent with the thermokarst ponds and localized subsidence observed around the instrument foundations (Figure A5, Appendix Figure A2 in original manuscript). Differences in benchmark stability may also contribute. The LVDT reference rods are anchored to depths of 30 m at SLC03 and 20 m at SLC07, whereas the foundations supporting the GNSS antenna and ultrasonic ranging sensor are anchored

to a depth of 6 m. Structural movement, including frost jacking, cannot be ruled out and is discussed further in Section 5.1.

5.1 Deployment and performance of the in-situ ground surface deformation monitoring system in permafrost terrain

Benchmark stability is a prerequisite for reliable monitoring of permafrost ground surface deformation. In our deployment, this requirement was addressed by anchoring steel rods or pipes deeply into the ground (e.g., 6 m for the GNSS antenna and ultrasonic ranging sensor foundations and 30 m for the LVDT reference rod, compared with an ALT of ~2.4 m). The larger subsidence rates observed by GNSS-IR and ultrasonic ranging relative to LVDT and InSAR may reflect pronounced thaw settlement associated with installation disturbance around these foundations, as shown by the field photographs in Appendix Figure A5 (Appendix Figure A2 in original manuscript). Benchmark-related effects, including frost jacking or residual instability of the shallower foundations, cannot be entirely excluded. Figure 8 shows that GNSS-IR and ultrasonic ranging exhibit smaller seasonal deformation amplitudes and larger subsidence trends than LVDT and InSAR. The foundations supporting the GNSS antenna and ultrasonic ranging sensor are anchored to a depth of 6 m. If these foundations move upward during winter, their movement could partially offset actual ground surface heave in the relative measurements, reducing the recorded seasonal amplitude. If they do not fully return to their previous elevations during thaw, residual uplift could accumulate over successive freeze–thaw cycles, making the ground surface appear progressively lower relative to the benchmarks and exaggerating apparent long-term subsidence. Notably, the discrepancy between GNSS-IR/ultrasonic ranging and LVDT/InSAR becomes more pronounced toward the end of the observation period, suggesting that benchmark-related effects may have increased over time. These potential effects should therefore be carefully considered when establishing long-term monitoring systems.

• Section 5: The in-situ techniques are quite well discussed but the value and limitations of InSAR are almost absent. At l.655, the regional scale is mentioned – this is only possible to get using remote sensing. Might be worth mentioning at the end of the discussion.

Following this suggestion, we have added the following discussion to **Section 5.1 Deployment and performance of the in-situ ground surface deformation monitoring system in permafrost terrain**:

Differences in spatial scale should therefore be considered when comparing LVDT with InSAR, which represents spatially averaged deformation over scales of approximately 10–100 m, or GNSS-IR, which has a footprint of approximately 50 m. In heterogeneous surface environments, observations with larger footprints integrate deformation across multiple microtopographic and subsurface settings, each characterized by different thawing and freezing onset times and seasonal amplitudes. The superposition of these local deformation processes smooths the signal and can obscure process-level features captured at a single point. Our comparison of LVDT and InSAR records shows that, although the two generally agree in long-term deformation trends and seasonal deformations, discrepancies remain in the onset and cessation of frost heave and thaw settlement (Figure 7a) and in seasonal amplitude in individual years. For example, during the 2023–2024 freeze–thaw cycle at SLC07, the LVDT record shows a marked increase in seasonal amplitude, whereas the InSAR-derived seasonal amplitude remains comparable to those of preceding years (Appendix Figure A4).

We have refined **Section 5.4 Deformation-based indicators of excess ground ice melt** and expanded the discussion of InSAR as follows:

Under such conditions, the multiannual subsidence trend may serve as a more robust indicator of the ground ice loss. InSAR provides a means of monitoring ground surface deformation over broad areas, and this study demonstrates that Sentinel-1 SBAS-InSAR can provide reasonably accurate deformation estimates in alpine meadow environments on the Tibetan Plateau. Sentinel-1 has accumulated approximately a decade of C-band SAR observations over many permafrost regions (Bartsch et al., 2026). Complementary L-band observations from NISAR offer the potential to extend deformation monitoring to more densely vegetated terrain, where C-band observations are particularly susceptible to decorrelation. In the Arctic, however, retrieving continuous multiannual deformation time series using InSAR is often challenging because winter snow cover and wet snow during spring snowmelt can cause strong decorrelation. In such cases, thaw-season deformation curves, along with interannual comparisons of thaw-season deformation processes, may still provide valuable information on excess ice melt.

• Same in the conclusion: there is a conclusion for all techniques, except InSAR.

The conclusions now include the following summary of the four monitoring methods:

The collocated observations provide a benchmark for evaluating the strengths and limitations of the four deformation monitoring methods and a foundation for integrated monitoring. All four methods show broadly consistent deformation patterns. InSAR provides long-term regional deformation time series and shows reasonably good agreement with LVDT measurements in the alpine meadow environment (Pearson r = 0.85 and RMSE = 13.02 mm at SLC03, r = 0.71 and RMSE = 20.0 mm at SLC07), with similar long-term trends and seasonal amplitudes. GNSS-IR and ultrasonic ranging are strongly correlated at SLC03 (r = 0.96; RMSE = 13.61 mm), although both may be affected by frost jacking of their shallower reference foundations at our site. The relatively limited snow cover on the Tibetan Plateau allows these methods to provide useful seasonal to multi-year deformation measurements, but measurement precision and data filtering constrain their ability to resolve detailed deformation processes on daily to weekly timescales.

Additional details:

• Title : the « : » after multi-year is not necessary.

We thank the reviewer for this editorial suggestion. After careful consideration, we would prefer to retain the colon, as it separates the temporal scope highlighted by "From sub-daily to multi-year" from the research topic and observational approach described in the remainder of the title.

• L.32: remove « - » after seasonal.

We have removed « - » after seasonal.

Original text: GNSS-IR and ultrasonic ranging are more affected by snow and vegetation and require substantial filtering, making them more suitable for seasonal- to multi-year monitoring than for resolving subtle sub-daily signals.

Revised text: GNSS-IR and ultrasonic ranging are more affected by snow and vegetation and require substantial filtering, making them more suitable for seasonal to multi-year monitoring than for resolving subtle sub-daily signals.

• L.40-49: could mention in this paragraph that this is valid for flat terrain. On slopes, other elements must be accounted for.

Thank you for this suggestion. We have revised the paragraph as follows.

Original text: Ground surface deformation in permafrost terrain is a key periglacial expression of coupled

thermal, hydrological, and mechanical processes within the active layer and underlying permafrost. At diurnal to seasonal timescales, deformation is mainly governed by frost heave and thaw subsidence associated with freeze–thaw cycling (J. Chen et al., 2020; Du et al., 2025; Smith, 1987). At multi-annual to decadal timescales, deformation reflects changes in ground ice storages: thaw of ice-rich permafrost and subsequent consolidation can produce persistent subsidence, whereas ground ice aggradation may lead to long-term surface uplift (Kokelj et al., 2007; Mackay & Burn, 2002; O'Neill & Burn, 2012; Shiklomanov et al., 2013; Streletskiy et al., 2025).

Revised text: Ground surface deformation in permafrost terrain is a key periglacial expression of coupled thermal, hydrological, and mechanical processes within the active layer and underlying permafrost. On flat terrain, vertical deformation at diurnal to seasonal timescales is mainly governed by frost heave and thaw subsidence associated with freeze–thaw cycling (J. Chen et al., 2020; Du et al., 2025; Smith, 1987). At multiannual to decadal timescales, vertical deformation in such terrain reflects changes in ground ice storage: thaw of ice-rich permafrost and subsequent consolidation can produce persistent subsidence, whereas ground ice aggradation may lead to long-term surface uplift (Kokelj et al., 2007; Mackay & Burn, 2002; O'Neill & Burn, 2012; Shiklomanov et al., 2013; Streletskiy et al., 2025). On slopes, gravity-driven downslope movements must also be considered when interpreting surface deformation (Reinosch et al., 2020), and thawing of ice-rich layers may enhance these movements by promoting basal soil shearing (Watine et al., 2025).

• L.48: 'integrates' is probably not the right word. 'is controlled by'?

We have revised the sentence as follows.

Original text: Ground deformation information is a sensitive observable for diagnosing permafrost responses to climate change, and useful for assessing associated hazards to infrastructure and slopes, as well as hydrological and ecological impacts linked to ground ice changes (Hjort et al., 2022; Kokelj et al., 2021; Nitzbon et al., 2020) as it integrates changes in temperature, phase state, water redistribution, and ground ice content.

Revised text: Ground deformation information is a sensitive observable for diagnosing permafrost responses to climate change, and useful for assessing associated hazards to infrastructure and slopes, as well as hydrological and ecological impacts linked to ground ice changes (Hjort et al., 2022; Kokelj et al., 2021; Nitzbon et al., 2020) as it is controlled by changes in temperature, phase state, water redistribution, and ground ice content.

• L.52: not only the Tibetan Plateau, all cold-climate regions with permafrost (mountains at lower latitudes).

We have revised the sentence as follows.

Original text: Continuous in situ deformation records are therefore essential, yet long, multi-annual records that capture complete freeze–thaw cycles remain rare in both the pan-Arctic and on the Tibetan Plateau permafrost regions.

Revised text: Continuous in situ deformation records are therefore essential, yet long, multi-year records that capture complete freeze–thaw cycles remain rare in both pan-Arctic permafrost regions and mountain permafrost regions at lower latitudes.

• L.52-53: 'To our knowledge, the work of Gruber (2020) remains…'

The wording has been corrected.

Original text: To our knowledge, work of (Gruber, 2020) remains one of the very few studies

Revised text: To our knowledge, work of Gruber (2020) remains one of the very few studies.

• L.61: space missing before 'Tilt-arm'.'…which are also contact in situ devices'

We have added a space before "Tilt-arm systems systems".

• L.69: 'larger than that of point sensors' could be removed (obvious in this sentence)

We have removed "larger than that of point sensors".

Original text: Global Navigation Satellite System Interferometric Reflectometry (GNSS-IR) has recently emerged as another promising technique, providing daily, and under suitable conditions sub-daily, deformation estimates over a footprint (from a few meters to several tens of meters) larger than that of point sensors.

Revised text: Global Navigation Satellite System Interferometric Reflectometry (GNSS-IR) has recently emerged as another promising technique, providing daily, and under suitable conditions sub-daily, deformation estimates over a footprint from a few meters to several tens of meters.

• L.73: 'limited to the work of Zhang et al. (2021)…'

The wording has been corrected.

Original text: On the Tibetan Plateau, applications remain especially scarce and, to our knowledge, are limited to work of (J. Zhang et al., 2021) in the northern plateau

Revised text: On the Tibetan Plateau, applications remain especially scarce and, to our knowledge, are limited

to work of Zhang et al. (2021) in the northern plateau.

• L.76: not clear what ‘spatial monitoring’ means. I believe it could be removed.

We have replaced “At broader scales and spatial monitoring” with “At broader scales”.

• L.76: InSAR acronym is never explained.

Thank you for pointing this out. We have provided the full form of InSAR and added a brief explanation of its underlying principle.

Original text: At broader scales and spatial monitoring, InSAR has become a primary tool for mapping seasonal and long-term permafrost deformation with millimetre- to centimetre-level precision (Z. Zhang et al., 2022; Zwieback, Liu, et al., 2024).

Revised text: At broader scales, interferometric synthetic aperture radar (InSAR) has become a primary tool for mapping seasonal and long-term permafrost deformation with millimeter- to centimeter-level precision (Z. Zhang et al., 2022; Zwieback, Liu, et al., 2024). It estimates ground displacement along the radar line of sight by analyzing phase differences between SAR images acquired over the same area at different times.

• L.92: ‘permafrost-deformation’ sounds a bit odd. It is not the permafrost itself that is deforming.

We have revised the sentence as follows.

Original text: To address these gaps, we established an intensively instrumented permafrost-deformation supersite in the central Tibetan Plateau

Revised text: To address these gaps, we established an intensively instrumented supersite on the central Tibetan Plateau to monitor ground surface deformation in permafrost terrain.

• L.95-96: the discrepancy between the start of the operation (2021) and the observation period used in the study (from 2022) is visible here but explained only later (l.141-142). You could consider simplifying here (for instance avoiding mentioning 2021) – it would be less confusing.

Thank you for this suggestion. To avoid confusion, the phrase “in operation since 2021” has been deleted.

Original text: a ground-based monitoring system integrating LVDT measurements, ultrasonic ranging, GNSS-IR, and multi-layer hydrothermal observations has been in operation since 2021.

Revised text: The ground-based monitoring system integrates LVDT measurements, ultrasonic ranging, GNSS-IR, and multi-depth soil temperature and moisture observations.

• L.96: SBAS-InSAR acronym not explained.

Thank you for this suggestion. In the Introduction, after introducing InSAR, we have added an explanation of SBAS-InSAR.

The added text reads: Among time-series InSAR approaches, small baseline subset InSAR (SBAS-InSAR) forms a network of interferograms from SAR image pairs with short temporal and small perpendicular baselines to mitigate temporal and spatial decorrelation (Berardino et al., 2002). This strategy facilitates deformation monitoring in permafrost terrain, where seasonal freeze–thaw processes and associated changes in surface scattering can cause substantial coherence loss.

• L.110: 'monument' is not the right word. Simply 'structure' would fit better. Check in the whole manuscript: 'monument' is used several times in this context (e.g., l.366: possible structural movement instead, and at l.562).

The original wording "GNSS antenna and its monument" has been revised to "GNSS antenna and its structure".

Other uses of "monument" have been replaced or rephrased as follows:

L64-65 Original text: By contrast, sonic ranging represents a non-contact approach. Originally developed for snow depth or water level measurements, they can also be used to monitor ground surface elevation change when mounted on stable monuments.

Revised text: By contrast, sonic ranging represents a non-contact approach. Originally developed for snow depth or water level measurements, this technique can also be used to monitor ground surface elevation change when mounted on stable structures.

L333-336 Original text: The larger GNSS-IR and ultrasonic ranging subsidence trends reflect stronger local thaw disturbance in their observation footprint, confirmed by thermokarst ponds and subsidence developed around their monuments, shown in Appendix Figure A2. In addition, the LVDT reference rod is anchored to 30 m depth, whereas the GNSS-IR and ultrasonic ranging structures are anchored to 6 m depth; possible monument movement, including frost jacking, cannot be fully ruled out and is discussed further in Section 5.1.

Revised text: The larger subsidence trends derived from GNSS-IR and ultrasonic ranging may reflect pronounced local thaw settlement associated with installation disturbance within their observation footprints. This interpretation is consistent with the thermokarst ponds and localized subsidence observed around the instrument foundations (Figure A5). Differences in benchmark stability may also contribute. The LVDT reference rods are anchored to depths of 30 m at SLC03 and 20 m at SLC07, whereas the foundations supporting the GNSS antenna and ultrasonic ranging sensor are anchored to a depth of 6 m. Structural movement, including frost jacking, cannot be ruled out and is discussed further in Section 5.1.

L562-563 Original text: The larger subsidence rates observed by GNSS-IR and ultrasonic ranging relative to LVDT and InSAR may reflect pronounced thaw settlement associated with installation disturbance around the GNSS antenna and ultrasonic ranging sensor monuments, as shown by the field photographs in Appendix Figure A2.

Revised text: The larger subsidence rates observed by GNSS-IR and ultrasonic ranging relative to LVDT and InSAR may reflect pronounced thaw settlement associated with installation disturbance around these foundations, as shown by the field photographs in Appendix Figure A5.

• L.122: to make it clear, add the name SLC03 in this sentence and refer to Fig. 1d.

We have revised the sentence as follows.

Original text: The supersite combines collocated LVDT-based measurements, ultrasonic ranging, and GNSS-IR observations of ground surface elevation change, complemented by Sentinel-1 InSAR over the surrounding region.

Revised text: The SLC03 supersite (Figure 1d) combines collocated LVDT measurements, ultrasonic ranging, and GNSS-IR to monitor ground surface elevation changes (Figure 1b), with Sentinel-1 InSAR providing complementary observations over the surrounding region.

• L.137: to make it clear here, refer to Fig. 1d at the end of the sentence.

We have revised the sentence as follows.

Original text: To capture spatial variability, an additional LVDT-based automated deformation monitoring system was deployed at a second borehole site (SLC07), located 10.6 km northwest of the main station (supersite SLC03).

Revised text: To capture spatial variability in ground surface deformation, an additional automated LVDT-based monitoring system was deployed at the SLC07 borehole site, approximately 11 km northwest of the SLC03 supersite (Figure 1d).

• L.125-127: refer to Fig. 1b-c at the end of the sentence

We have added references to Fig.1 and Fig. 1c.

Original text: In November 2021, a meteorological and permafrost monitoring station was installed, equipped with a GNSS receiver (Trimble NetR9), an automated ground surface deformation monitoring system, and active-layer hydrothermal sensors initially spanning depths of 5–50 cm

Revised text: A meteorological and permafrost monitoring station was established at the site in November 2021, equipped with a GNSS receiver (Trimble NetR9) (Figure 1c), an automated ground surface deformation monitoring system, and soil temperature and moisture sensors initially installed at depths of 5–50 cm within the active layer (Figure1 b).

• L.131: missing space after 'Table 1'.

We have added a space after "Table 1".

• L.146-158: half of this paragraph uses past tense, the other half uses present tense. I would suggest harmonizing to 'present'– lighter and the sensor is indeed still operating, I guess.

Thank you for this suggestion. The paragraph now consistently uses the present tense. The revised paragraph is as follows:

The developed automated deformation monitoring system consists of an LVDT displacement sensor, a data transfer unit (DTU) for remote telemetry or a datalogger for local storage, and a solar power supply, shown in Figure 2. The LVDT sensor used in this study has a measurement range of 150 mm, a linearity error of ≤ 0.25 % of full scale, and a manufacturer-specified repeatability of 0.01 mm. The LVDT sensor is installed adjacent to a steel reference rod anchored deeply into the ground (30 m for SLC03 and 20 m for SLC07), which serves as a stable benchmark. The lower end of the sensor is connected to a perforated footplate resting on the ground surface. The footplate is 8 cm in diameter and moves vertically with the ground surface during heave and subsidence. Multiple holes in the footplate allow water and air exchange with the underlying soil while minimizing disturbance to surface energy and moisture fluxes (Figure 2c). Because the footplate remains in

direct contact with the ground surface beneath snow and vegetation (Figure 2d), the measurements are less affected by changes in surface cover than those obtained using non-contact methods. The LVDT sensor converts the relative motion of its ferromagnetic core, driven by vertical movement of the footplate, into a digital displacement signal. This signal is transmitted via Modbus RTU over an RS-485 interface. At SLC03, where network coverage is available, measurements are uploaded to a remote server via the mobile network using the data transfer unit (DTU). When network connectivity is unavailable, the data are stored locally on a datalogger.

• L.198: reference to A/φ could be added in paratheses.

To improve readability and help readers relate the text to the equation, we have formatted A φ and the other mathematical symbols in italics in the text.

GNSS-IR infers surface elevation changes from interference between direct and ground-reflected GNSS signals recorded in signal-to-noise ratio (SNR) observations. The dominant frequency component f (Hz) can be extracted from the SNR using Lomb-Scargle Periodogram (LSP) analysis which can be expressed as:

$$SNR = A(e)\, sin(2\pi f\, sin\, e + \phi(e)) \quad (1)$$

Where $A(e)$ and $\phi(e)$ represent the oscillation amplitude and phase offset varying with satellite elevation angle e (degrees). The reflector height h can be determined based the relationship between reflector height and dominant frequency component $f = 2h / \lambda$. h (meters) is the reflector height denoting the distance of ground surface relative to receiver, λ (meters) is the GNSS signal wavelength.

• L.199-200: revise this sentence. 'The reflector height h can be determined based on the relationship between the reflector height and the dominant frequency:equation'.

We have revised the sentence as follows.

Original text: Based the relationship between reflector height and dominant frequency component f = 2h/λ, the reflector height h can be determined.

Revised text: The reflector height h can be determined based the relationship between reflector height and dominant frequency component $f = 2h / \lambda$.

• L.242-249: partly a repetition compared to the method section (3.4). Some of the info here could be moved to methods, I think.

Thank you for this suggestion. We have moved this material to Section 3.4 Sentinel-1 SBAS-InSAR ground surface deformation monitoring. **The revised section**, incorporating this material, reads in full as follows:

Sentinel-1 SBAS-InSAR processing was applied to derive ground surface deformation over the area surrounding the in situ monitoring site. A total of 250 Sentinel-1 SLC acquisitions were obtained in interferometric wide-swath mode along the ascending track (Path 41) between 5 August 2017 and 15 November 2025. Interferograms were generated by pairing each SAR acquisition with its next two acquisitions (t – t+1 and t – t+2), with temporal baselines generally ranging from 12 to 24 d and occasionally extending to 36 d. This pairing strategy yielded a total of 497 interferometric pairs. SBAS-InSAR processing was performed using ISCE2 and MintPy. During processing, 10 looks in range and 2 looks in azimuth were applied to reduce noise and produce an approximately square grid (finally geocoded to 40 m grid). Differential phases were unwrapped using the SNAPHU minimum cost flow algorithm (C. W. Chen & Zebker, 2002), and the interferogram network was inverted into a deformation time series using a weighted least-squares approach. Following time-series inversion, phase deramping and correction for residual topographic errors were applied. The deformation time series was then smoothed using a three-acquisition moving average, with a nominal window length of 36 d (occasionally 48 d). Further details of the SBAS-InSAR processing workflow are provided in our previous study (Wang et al., 2022). Because the terrain is relatively flat and deformation is expected to be dominated by freeze-thaw-related vertical motion, line-of-sight (LOS) deformation was converted to vertical displacement by dividing by the cosine of the incidence angle, assuming negligible horizontal motion.

In the study area, the land surface is covered by alpine meadow in summer, while winter snow cover is generally thin and short-lived. The relatively sparse vegetation and limited snow cover help maintain relatively high coherence throughout the year in C-band interferometric pairs with temporal baselines of up to one month. Across the 497 interferograms, mean coherence ranges from 0.59 for the 20230506–20230530 interferometric pair to 0.99 for the 20230915–20230927 pair, with 464 interferograms having a mean coherence greater than 0.8. All 497 interferograms are retained in the analysis. Their coherence distribution is presented in Appendix Figure A3.

Surface deformation was estimated relative to a reference point that maintained a mean interferometric coherence of 0.99 across all interferometric pairs and was located on a small hill approximately 5 km from

SLC03 and 11 km from SLC07 (Figure 3a, 3b). Given this spatial proximity, subtracting the deformation at the reference point helped reduce the influence of common atmospheric artefacts and potential regional crustal motion in the deformation time series at the monitoring sites.

• L.251: 'Combined to Figure 1d, the spatial pattern shown in Figure 3a-b…' Very hard to relate cause the extent is not the same. A rectangle showing the extent of Fig.3 on Fig.1d would help. But ideally, it would be best to have the same extent as 1d on Fig.3, in order also to include the second site SLC07.

We have followed this suggestion and redrawn Fig. 1d and Fig. 3ab to have the same extent as Fig. 1d on Fig. 3. The revised Fig. 1 and Fig. 3 are provided below.

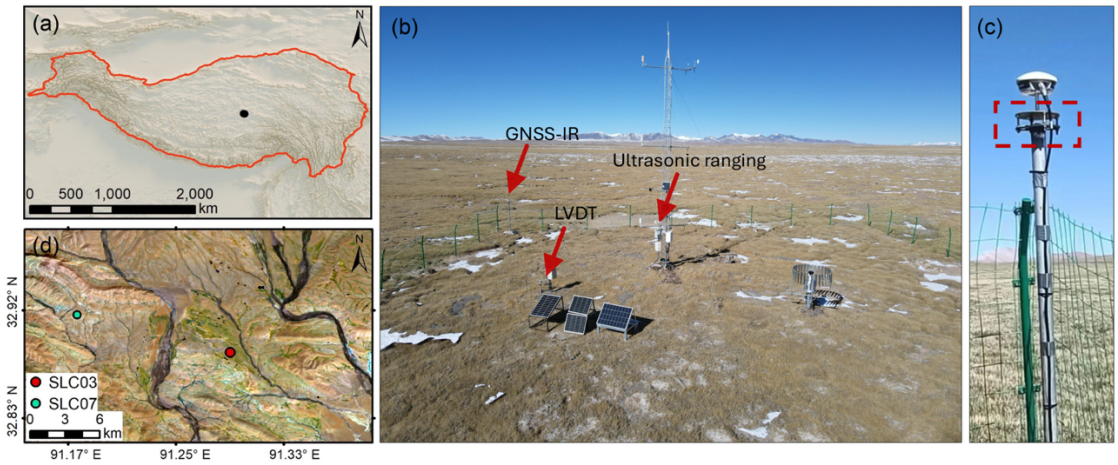


Figure 1. Study area and measurements. (a) Location of the study area on the Tibetan Plateau. (b) Instrument layout at the meteorological and permafrost monitoring station of SLC03, showing the three ground-based deformation monitoring systems (GNSS-IR, ultrasonic ranging, and LVDT) and the surrounding alpine swamp meadow. (c) GNSS antenna and its supporting structure at SLC03. The red rectangle highlights the levelling mount used to keep the GNSS antenna level. (d) Locations of the two automated LVDT-based in situ ground surface deformation monitoring sites.

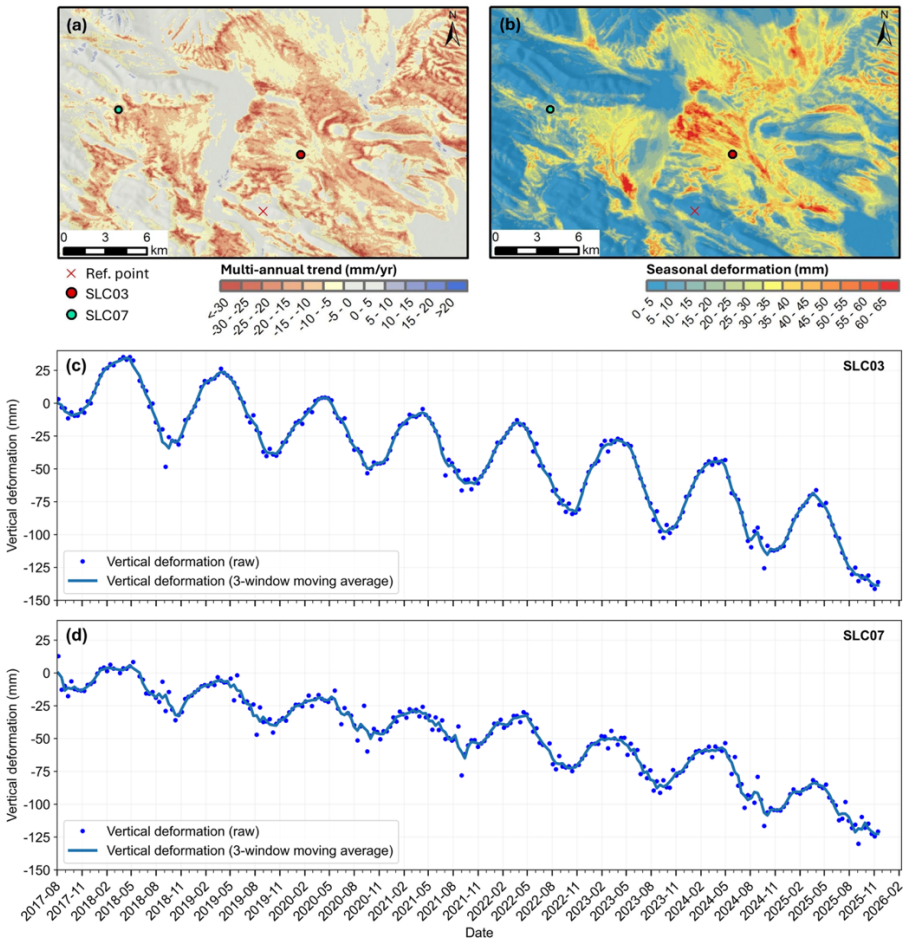


Figure 3. Sentinel-1 InSAR-derived deformation. Spatial distributions of (a) the long-term deformation trend and (b) seasonal deformation (peak-to-peak) in the radar line-of-sight (LOS) direction, shown over a hillshade basemap. (c–d) Vertical deformation time series at SLC03 and SLC07, respectively.

• L.283: specify when (May) the settlement begins.

We have specified the timing when the settlement begins.

Original text: During thaw, settlement also begins earlier at SLC07, whereas at SLC03 the onset of rapid settlement is delayed until June in some years.

Revised text: During the thaw season, pronounced and sustained settlement also began earlier at SLC07, around mid-May, whereas at SLC03 the onset of rapid settlement is delayed until end of May and June in some years.

• L.285: remove ‘also’– not really comparable with the previous sentence.

We have removed the word “also”.

Original text: At SLC03, a late-thaw-season breakpoint followed by accelerated subsidence is also observed in 2022, 2024, and 2025, and is particularly pronounced in 2024.

Revised text: At SLC03, a late-thaw-season breakpoint followed by accelerated subsidence is observed in 2022, 2024, and 2025, and is particularly pronounced in 2024.

• L.295: I don't think 'positive excursions' is a classical terminology: outliers instead? Check in the whole manuscript: 'excursion' is used several times in this context (e.g., l.307, l.547).

The term "positive excursions" has been replaced in the manuscript as follows:

Original text at L295: In the raw series, numerous short-lived positive excursions occur throughout the record.

Revised text: In the raw series, numerous short-lived upward spikes occur throughout the record.

Original text at L305: Orange markers indicate observations flagged as spikes, corresponding to short-lived upward excursions (mainly caused by snow) in the raw series.

Revised text: Orange tick marks at the top indicate the timing of observations flagged as short-lived upward spikes, mainly associated with snow.

Original text at L547: in the ultrasonic record, snow accumulation appears as episodic positive excursions rather than as a persistent winter surface

Revised text: In the ultrasonic record, snow accumulation appears as episodic positive outliers rather than as a persistent signal

• L.311: The measured cumulative lowering is not mentioned systematically for all techniques, it would be nice to add it for the others (for sake of comparison).

Thank you for this suggestion. We have added cumulative deformation values for each monitoring method to facilitate comparison.

In Section 4.1.1 Ground surface deformation from Sentinel-1 InSAR, we have added the following statements:

"The smoothed vertical InSAR time series are divided into two intervals of approximately 4 years each, with 25 September 2021 as the temporal midpoint. At SLC03, the deformation rate changes from approximately −13.65 mm yr^{-1} during the earlier interval to −18.95 mm yr^{-1} during the later interval. At SLC07, the corresponding rates are −11.68 and −16.49 mm yr^{-1}, respectively. Compared with the earlier interval, subsidence rates in the later interval are approximately 39 % higher at SLC03 and 41 % higher at SLC07, indicating more

rapid surface lowering during the more recent monitoring period. The modelled seasonal deformation increases from 51.38 to 58.12 mm at SLC03 and from 24.51 to 30.95 mm at SLC07, corresponding to increases of approximately 13.1 % and 26.3 %, respectively."

In section 4.1.2 Ground surface deformation from LVDT-based measurements, we have added the following statements:

"With 18 June 2022 as the reference date, the thaw-season minimum deformation at SLC03 becomes progressively more negative, decreasing from approximately −58 mm in 2022 to −75 mm in 2023 and −109 mm in 2025. At SLC07, the minimum decreases from approximately −22 mm in 2022 to −30 mm in 2023 and −42 mm in 2024."

In section 4.1.3 Ground surface deformation from ultrasonic ranging, we have added the following statements:

"Relative to the common reference date of 18 June 2022, the minimum thaw-season deformation derived from ultrasonic ranging decreases from approximately −67 mm in 2022 to −101 mm in 2023, −130 mm in 2024, and −153 mm in 2025."

In Section 4.1.4 Ground surface deformation from GNSS-IR, we have added the following statements:

"With 18 June 2022 as the common reference date, the minimum thaw-season deformation derived from GNSS-IR decreases from approximately −72 mm in 2022 to −95 mm in 2023 and −132 mm in 2024. By 8 September 2025, the deformation had reached −154 mm, although this value may not represent the minimum for the 2025 thaw season."

• L.320: (iv) late-winter freezing

We have changed "(iv) Late-winter freezing" to "(iv) late-winter freezing".

• L.326: 'early part of the AF stage' / 'settlement still persists'

We have replaced "early part of AF stage" with "early part of the AF stage" and "thaw settlement still persist" with "settlement still persists".

• L.359: here short temporal baselines are mentioned but never explained before.

Thank you for this suggestion. In the Introduction section, we have added an explanation of SBAS-InSAR: Among time-series InSAR approaches, small baseline subset InSAR (SBAS-InSAR) forms a network of interferograms from SAR image pairs with short temporal and small perpendicular baselines to mitigate temporal and spatial decorrelation (Berardino et al., 2002).

• L.394: bug of font size

Thank you for pointing this out. We have made the font size consistent.

• L.400: might consider weakening this statement a bit. It might look less obvious due to different scales (faster movement) but in reality the stepwise pattern is also clear in October.

We agree with the reviewer and have softened the statement as follows.

Original text: This interval therefore represents a late-thaw-season deformation regime characterized by continuous subsidence.

Revised text: This late-thaw-season interval shows sustained subsidence at a relatively high rate.

• L.408: 'this layer froze during this period'

We have revised the wording as follows.

Original text: indicating that this depth froze during the period.

Revised text: indicating that this layer froze during this period

• L.408-409: 'freeze-back'

We have replaced the word "freeze back" with "freeze-back"

• L.415: 'freezing front advance'

We have replaced "slower freezing-front advance" with "slower freezing front advance".

• L.455: '…and, in some year, a lag is visible compared to the surface thaw onset.'

We have revised the sentence as follows.

Original text: The onset of significant thaw settlement differs among years and, in some years, lags the onset of

surface thaw.

Revised text: The onset of significant thaw settlement differs among years and, in some years, a lag is visible compared to the surface thaw onset.

• L. 458: the Stefan equation is never introduced. Add a reference in Section 3.5?

Thank you for this suggestion. At the end of Section 3.5, we have added an explanation of the Stefan equation as follows:

Daily air temperature was used to calculate accumulated degree days of thawing (DDT) and freezing (DDF). Thawing and freezing onset were defined as the first day when the daily mean air temperature remained above or below 0 °C for seven consecutive days. Accumulated thermal forcing can be related to thawing or freezing depth through the classical Stefan equation under idealized assumptions of one-dimensional conductive heat transfer, constant soil properties, and negligible sensible heat storage (Kurylyk and Hayashi, 2016). This relationship can be expressed as

$$z(t) = C\sqrt{I(t)} \quad (2)$$

where $z(t)$ is the depth of the thawing or freezing front, $I(t)$ is the accumulated ground surface thawing or freezing index expressed as a positive magnitude, and C depends on soil thermal conductivity and volumetric latent heat. Accordingly, DDT and DDF, calculated here using air temperature as a proxy for ground surface thermal forcing, provide approximate indicators of thawing and freezing progression, respectively.

• L.460: I don't think it is possible to say 'steepest proportionality'

For clarity, we have revised the sentence as follows.

Original text: Among the four thaw seasons, year 2023 shows the steepest proportionality, which means the highest apparent settlement efficiency relative to cumulative thawing.

Revised text: Among the four thaw seasons, the 2023 season exhibited the most negative regression slope, indicating the greatest apparent settlement per unit increase in $\sqrt{\text{TDD}}$.

• L. 472: active layer is more usually written without a '-' Check the entire text, it is inconsistent.

Thank you for this suggestion. We have checked the entire manuscript and now consistently write active layer without a "-".

• L.478: ‘indicators of ground ice melt’: early season subsidence is also an indicator of ground ice melt, just not at the same depth. Consider rephrasing to ‘indicators of top-of-permafrost ice melt’

Thank you for this suggestion, which makes the interpretation more precise. We have revised the title of Section 4.4.2 from “Late-thaw-season subsidence and indicators of ground ice melt” to “Late-thaw-season subsidence and indicators of top-of-permafrost ice melt”.

• L.487-488: ‘shallower than in the other years’: nice to include the values for the other years. Reference to figure 7e?

We have revised the sentence as follows.

Original text: Extrapolation of the temperature profile suggests a maximum thaw depth of only about 230 cm, far shallower than in the other years.

Revised text: The soil moisture profiles suggest that thaw likely did not reach 240 cm in 2023, whereas they clearly indicate thawing at this depth in 2022 and 2024 (Figure 7c). Extrapolation of the soil temperature profiles suggests maximum thaw depths of approximately 260 cm in 2022 and 2024, at least 20 cm greater than in 2023 (Figure 7e).

• L.490: good to also refer to the full time series (figure 10g).

Thank you for this suggestion. We have highlighted this interval with a red dashed box in Figure 10g and added the following reference to the full time series.

Original text: Figure 11 shows ground deformation and deep hydrothermal profiles from 11 September to 4 October 2024, spanning the period during which the acceleration breakpoint occurred.

Revised text: Figure 11 shows ground deformation and deep soil temperature and moisture profiles from 11 September to 4 October 2024, a period encompassing the subsidence acceleration breakpoint. This interval is highlighted by a red dashed box in the full time series for the 2024 thaw season (Figure 10g).

• L.514: missing a mention to the year (2024) in first sentence. Or if this refers to all years, it should be modified as: ‘Distinct slight heave events were observed in…’

Thank you for this suggestion. We have revised the sentence as follows.

Original text: A distinct slight heave event was observed in late April to early May at both SLC03 and SLC07 Figure 4).

Revised text: Small but distinct heave events are observed at both sites between mid-April and early May, including at SLC03 in 2024 and 2025 and at SLC07 in 2022–2024 (Figure 4).

• L.524: might try to find another word that 'dip'– unclear.

We have replaced "dip" with an alternative expression.

Original text: This late-winter "dip" likely reflects the same underlying process, namely thawing and refreezing of infiltrated water.

Revised text: This "shallow trough" in the late-winter deformation record may likewise reflect alternating thawing and refreezing associated with infiltrated water.

• L. 528: high accuracy, high temporal resolution'

We have revised the wording as follows.

Original text: This study demonstrates a practical and deployable approach for high-accuracy, high-temporal-resolution continuous monitoring of permafrost ground surface deformation using an LVDT sensor–logger configuration.

Revised text: This study demonstrates a practical and deployable approach for high accuracy, high temporal resolution continuous monitoring of permafrost ground surface deformation using an LVDT sensor–logger configuration.

• L.546-548: Long sentence. Consider splitting in 3 sentences: 'In the interior Tibetan Plateau, winter snow cover if often thin, and short-lived so snow does not permanently obscure the ground surface. In the ultrasonic record, snow accumulation appears as episodic positive outliers rather than as a persistent signal (as shown in Figure 5). With appropriate filtering, most of the underlying deformation signal can be recovered.'

Thank you for this suggestion. We have divided the long sentence into shorter sentences.

Original text: In the interior Tibetan Plateau, winter snow cover is often thin, and short-lived, so snow does not permanently obscure the ground surface, thus in the ultrasonic record, snow accumulation appears as episodic positive excursions rather than as a persistent winter surface (as shown in Figure 5), and with appropriate filtering most of the underlying deformation signal can be recovered.

Revised text: In the interior Tibetan Plateau, winter snow cover is often thin, and short-lived so snow does not permanently obscure the ground surface. In the ultrasonic record, snow accumulation appears as episodic positive outliers rather than as a persistent signal (as shown in Figure 5). With appropriate filtering, most of the underlying deformation signal can be recovered.

• L.563: remove 'However'.

We have removed "However".

• L.570: 'failure of the deepest sensors': this info is missing in the methods section.

In Section 3.5 Meteorological and active layer hydrothermal monitoring, we have specified the measurement depths and clarified the sensor-related data gaps and limitations as follows:

"These observations include air temperature at 2 m, precipitation, soil temperature (ST), and soil volumetric water content (VWC). ST and VWC are monitored at the same depths of 5, 10, 20, 40, 60, 80, 120, 160, 180, 200, 220, and 240 cm below the ground surface.

Gaps in the ST and VWC records occur from 23 January to 4 April 2025 and from 13 August to 8 November 2025. During these periods, missing ST values at 5 cm were filled using regression-based estimates derived from a separate temperature record obtained with a sensor temporarily installed at the same depth. At 240 cm depth, ST and VWC observations are sparse from 18 May to 25 November 2023. Although daily values are available, some are based on very few valid 10-minute observations. Despite the relatively small diurnal variations in temperature and moisture at this depth, sparse sampling may still introduce bias into the daily means."

• L576: 'details'.

We have replaced "detail" with "details".

• L.583: 'soil temperature, moisture profiles and…'

We have revised the wording as follows.

Original text: The sub-daily deformation record, combined with soil temperature and moisture profiles and snow information

Revised text: The sub-daily deformation record, combined with soil temperature, moisture profiles and snow

information

• L597: start a new sentence after ‘a few millimetre.’

Thank you for this suggestion.

The original passage is: Earlier studies from the Canadian and Colorado Rockies have shown that diurnal freeze–thaw deformation is predominantly a near-surface process (Fahey, 1973; Smith, 1987), generally confined to the upper 10 cm of soil, with typical vertical displacements of only a few millimeters; accordingly, its geomorphic significance is thought to be largely limited to micro-scale surface disturbance rather than the development of large-scale periglacial landforms.

The diurnal frost-heave and thaw-settlement signals analyzed in the original manuscript (~0.1 mm) are very small and comparable in magnitude to displacement associated with thermal expansion and contraction of the sensor. Given these small amplitudes and the sensor’s measured temperature sensitivity, we have tempered the interpretation of these signals in the revised manuscript and removed the passage quoted above.

• L.606: ‘in overall process shape’? Not sure what it means.

For clarity, we have removed this expression and revised the passage as follows.

Original text: show marked differences in seasonal deformation amplitude, in the onset timing of thaw settlement and freeze-back heave, and in overall process shape (Figure 4).

Revised text: exhibited marked differences in seasonal deformation amplitude and the onset of thaw settlement and freeze-back heave (Figure 4).

• L.611: ‘the timing of the thaw settlement’.

We have revised the wording from “The timing of thaw-settlement onset also varied among years” to “The onset of thaw settlement also varied among years”.

• L.630: ‘smooth’ instead of ‘clean’?

We now use “smooth” instead of “clean”.

Original text: By comparison, the deformation series at both of our sites are comparatively “clean”, with weak short-term fluctuations.

Revised text: By comparison, the deformation series at both of our sites are comparatively smooth, with weak short-term fluctuations.

• L.632: 'organic layer thickness?, without '-'

We have replaced "organic-layer thickness" with "organic layer thickness".

• L.641: when the thaw front reached…'

We have replaced "When thaw reaches ice-supersaturated material" with "When the thaw front reaches ice-supersaturated material"

• L.644: 'signature of thaw front reaching the ice-rich permafrost'.

We have replaced "signature of thaw engaging ice-rich permafrost" with "signature of thaw front reaching the ice-rich permafrost".

• L.646: might be wise to repeat that it is because 2023 is a cold year.

Thank you for this suggestion. We have revised the sentence to restate that 2023 was relatively cold.

Original text: In our record, such breakpoint-style acceleration is evident in year 2022 (20220926), 2024 (20240921), and 2025 (20251006), but not in 2023.

Revised text: In our record, such acceleration is evident in year 2022 (20220926), 2024 (20240921), and 2025 (20251006), but not in 2023, a relatively cold year with the lowest TDD among the four years (Figure 7d).

• L.654: 'the cumulative deformation legacy of ground ice loss'? Not sure to understand the phrasing. Simply 'indicator of the ground ice loss' would be clearer.

Thank you for this suggestion. We have simplified the wording.

Original text: Under such conditions, the multiannual subsidence trend may provide a more robust outcome indicator of the cumulative deformation legacy of ground ice loss.

Revised text: Under such conditions, the multiannual subsidence trend may serve as a more robust indicator of the ground ice loss.